Report Prepared by:

Kingsley Lau and
Alberto A. Sagüés

CORROSION EVALUATION OF BRIDGES WITH EPOXY-COATED REBAR

Contract No. BD544-23
Final Report to Florida Department of Transportation

A. A. Sagüés
Principal Investigator
Department of Civil and Environmental Engineering

UNIVERSITY OF SOUTH FLORIDA
Tampa, FL 33620
February 28, 2009

Technical Report Documentation Page

1. Report No.	2. Government Accession No.	3. Recipient's Catalog No.
BD544 - 23		

4. Title and Subtitle	5. Report Date
CORROSION EVALUATION OF BRIDGES WITH EPOXY-COATED REBAR	February 28, 2009
	6. Performing Organization Code

7. Author(s)	8. Performing Organization Report No.
K. Lau and A. A. Sagüés	

9. Performing Organization Name and Address	10. Work Unit No. (TRAIS)
Department of Civil and Environmental Engineering University of South Florida Tampa, FL 33620	11. Contract or Grant No. BD544 - 23

12. Sponsoring Agency Name and Address	13. Type of Report and Period Covered
Florida Department of Transportation 605 Suwannee St. MS 30 Tallahassee, Florida 32399 (850)414-4615	Final Report 11/01/2004 - 2/28/2009
	14. Sponsoring Agency Code

15. Supplementary Notes

Prepared in cooperation with the USDOT and FHWA

16. Abstract

Epoxy coated steel reinforcement (ECR) was used for corrosion control in FDOT marine reinforced concrete bridges from the late 1970's up to the early 1990's. However, severe ECR corrosion developed in some Florida Keys Bridges. Investigations completed in 1993 showed that those structures had concrete with high permeability. Early models projected corrosion development of other FDOT ECR structures with moderate concrete permeability after one more decade or so, and lesser likelihood of observing corrosion at that in other bridges with lower concrete permeability. This investigation examined the present corrosion condition of 13 ECR structures to validate and refine those earlier projections. Damage was found to have progressed steadily in the bridges showing early corrosion. Externally recognizable ECR corrosion damage was found, as expected, in other bridges with intermediate concrete permeability. No severe ECR corrosion developed when the coated bar was protected by a thick cover of sound, very low permeability concrete as encountered in very low concrete permeability bridges. However, there was widespread disbondment of the epoxy coating in all these structures even in sound concrete locations. This disbondment together with observed frequent coating breaks are expected to facilitate corrosion initiation as chloride levels at the rebar depth increase in future decades. Severe corrosion was also absent from locations in two low concrete permeability bridges where preexisting concrete cracks had allowed localized chloride ion penetration. However, in another low permeability concrete bridge in this group (Howard Frankland) significant ECR corrosion was observed at previously cracked concrete locations where the crack intersected the rebar. This observation is an important warning of potentially severe local damage in the future. Frequent monitoring of these and similar locations is advisable. An improved durability projection model was applied to improve ECR corrosion performance predictions in sound concrete. Electrochemical Impedance Spectroscopy (EIS) measurements of ECR in extracted cores showed good potential for non destructive characterization of the extent of coating damage. The technical content of this investigation is closely supplemented by that of the companion FDOT project, "Corrosion of Steel in Locally Deficient Concrete", BD544-31.

17. Key Words	18. Distribution Statement
Epoxy coated rebar, corrosion, bridges, Florida Keys, concrete cracking, durability forecasting.	No Restriction This report is available to the public through the NTIS, Springfield, VA 22161

19. Security Classif. (of this report)	20. Security Classif. (of this page)	21. No. of Pages	22. Price
Unclassified	Unclassified	59	

DISCLAIMER

The opinions, findings, and conclusions expressed in this publication are those of the authors and not necessarily those of the State of Florida Department of Transportation.

SI* (MODERN METRIC) CONVERSION FACTORS

APPROXIMATE CONVERSIONS TO SI UNITS

Symbol	When You Know	Multiply By	To Find	Symbol
		LENGTH		
in	inches	25.4	millimeters	mm
ft	feet	0.305	meters	m
yd	yards	0.914	meters	m
mi	miles	1.61	kilometers	km
		AREA		
in^2	square inches	645.2	square millimeters	mm^2
ft^2	square feet	0.093	square meters	m^2
yd^2	square yard	0.836	square meters	m^2
ac	acres	0.405	hectares	ha
mi^2	square miles	2.59	square kilometers	km^2
		VOLUME		
fl oz	fluid ounces	29.57	milliliters	mL
gal	gallons	3.785	liters	L
ft^3	cubic feet	0.028	cubic meters	m^3
yd^3	cubic yards	0.765	cubic meters	m^3
		NOTE: volumes greater than 1000 L shall be shown in m^3		
		MASS		
oz	ounces	28.35	grams	g
lb	pounds	0.454	kilograms	kg
T	short tons (2000 lb)	0.907	megagrams (or "metric ton")	Mg (or "t")
		TEMPERATURE (exact degrees)		
°F	Fahrenheit	5 (F-32)/9 or (F-32)/1.8	Celsius	°C
		ILLUMINATION		
fc	foot-candles	10.76	lux	lx
fl	foot-Lamberts	3.426	$candela/m^2$	cd/m^2
		FORCE and PRESSURE or STRESS		
lbf	poundforce	4.45	newtons	N
lbf/in^2	poundforce per square inch	6.89	kilopascals	kPa

APPROXIMATE CONVERSIONS FROM SI UNITS

Symbol	When You Know	Multiply By	To Find	Symbol
		LENGTH		
mm	millimeters	0.039	inches	in
m	meters	3.28	feet	ft
m	meters	1.09	yards	yd
km	kilometers	0.621	miles	mi
		AREA		
mm^2	square millimeters	0.0016	square inches	in^2
m^2	square meters	10.764	square feet	ft^2
m^2	square meters	1.195	square yards	yd^2
ha	hectares	2.47	acres	ac
km^2	square kilometers	0.386	square miles	mi^2
		VOLUME		
mL	milliliters	0.034	fluid ounces	fl oz
L	liters	0.264	gallons	gal
m^3	cubic meters	35.314	cubic feet	ft^3
m^3	cubic meters	1.307	cubic yards	yd^3
		MASS		
g	grams	0.035	ounces	oz
kg	kilograms	2.202	pounds	lb
Mg (or "t")	megagrams (or "metric ton")	1.103	short tons (2000 lb)	T
		TEMPERATURE (exact degrees)		
°C	Celsius	1.8C+32	Fahrenheit	°F
		ILLUMINATION		
lx	lux	0.0929	foot-candles	fc
cd/m^2	$candela/m^2$	0.2919	foot-Lamberts	fl
		FORCE and PRESSURE or STRESS		
N	newtons	0.225	poundforce	lbf
kPa	kilopascals	0.145	poundforce per square inch	lbf/in^2

*SI is the symbol for the International System of Units. Appropriate rounding should be made to comply with Section 4 of ASTM E380.

EXECUTIVE SUMMARY

Note: The technical content of this investigation is closely supplemented by that of the companion FDOT project, "Corrosion of Steel in Locally Deficient Concrete", BD544-31. To best use available resources, field surveys and related analysis were conducted concurrently for both projects. For contractual reporting purposes the findings under both projects are reported in separate documents. However, for technical discussion and elaboration of conclusions it has been often necessary to refer to and reproduce here some of the material from the Final Report for Project BD544-31, cited accordingly. It is recommended that both documents be consulted for an integral view of the issues concerned.

Epoxy coated steel reinforcement (ECR) was used for corrosion control in approximately 300 Florida Dept. of Transportation (FDOT) marine reinforced concrete bridges from the late 1970's up to the early 1990's. The use of ECR for new FDOT structures was discontinued upon mounting evidence of severe corrosion in some of the existing bridges in the Florida Keys.

Earlier investigations completed in 1993 assessed the corrosion condition of 20 FDOT ECR bridges after ~5-12 years of service. Durability prognosis evaluations were formulated based on the research findings and application of an initiation-propagation deterioration model. The structures showing early corrosion had been found to have concrete with high permeability. Based on measured concrete properties indicative of permeability, mainly the chloride ion diffusivity , the model projected development of corrosion after about one more decade of service (that is, at the beginning of this investigation) in some additional FDOT ECR structures with moderate permeability. The projections indicated a lesser likelihood of observing corrosion at that in other bridges with lower concrete permeability. This investigation examined the present corrosion condition of those structures to validate and refine those earlier projections. Attention was given also to the possible effect of thin structural cracks on early corrosion in low permeability concrete. The information was used to improve predictive corrosion performance models and provide information suitable for evaluating future repair needs and assisting in formulating future maintenance strategies.

Tasks conducted toward those objectives included assessing the present ECR condition in 13 FDOT marine bridges by detailed examination in the field and in the laboratory plus corrosion records of other 5 bridges, evaluating the information to develop an updated corrosion forecasting model, and apply the model to obtain a prognosis for future corrosion development in existing ECR bridges. The bridges considered were classified into 4 groups. Group 1 included Florida Keys structures with documented severe early ECR corrosion during the 1991-93 investigation, to serve as a baseline. Group 2 consisted of bridges not

showing corrosion in 1991-3 but determined to have a high likelihood of ECR corrosion development during the following decade based on high chloride ion diffusivity. Group 3 included structures with overall low to very low chloride diffusivity but where some narrow cracks have been detected that permit fast localized chloride ingress, and Group 4 consisted of bridges with intermediate chloride diffusivity with some chances of ECR corrosion development at present.

The investigation showed that damage from corrosion of ECR has continued to develop steadily in the substructure of the Group 1 bridges, with no indication of slowdown. Externally recognizable ECR corrosion damage began to be noticeable at four Group 2 bridges ~2 decades after construction and continuing into the 3rd decade.

No severe ECR corrosion developed in situations where the coated bar was protected by a thick cover of sound, very low permeability concrete as encountered in Group 3 bridges. This confirmed previous modeling projections based on the very low chloride permeability of the sound concrete in these bridges. However, there was widespread disbondment of the epoxy coating in all these structures even in sound concrete locations. This disbondment together with observed frequent coating breaks are expected to facilitate corrosion initiation as chloride levels at the rebar depth increase in future decades. Severe corrosion was also absent from locations in two of the Group 3 bridges where preexisting concrete cracks had allowed localized chloride ion penetration. However, in the other bridge in this group (Howard Frankland) significant ECR corrosion was observed at previously cracked concrete locations where the crack intersected the rebar. The observation of ECR corrosion at cracked locations of a low permeability concrete bridge is an important warning of potentially severe local damage in the future. Frequent monitoring of these and similar locations is advisable, as is the development of predictive models for corrosion of ECR in locally deficient concrete.

A predictive ECR corrosion model was applied that replicated most of the damage function features observed in the field. The model divides the substructure in separate elements with individual chloride exposure, concrete permeability, concrete rebar cover, and extent of ECR coating imperfections.

The experimental results and predictive model calculations indicate that the propagation stage of corrosion dominated damage development in the structures that showed early deterioration. Significant corrosion of even a relatively small fraction of the rebar assembly could manifest itself as extensive and conspicuous damage, which can continue increasing for many years. The model projections account for the observed later development of corrosion in Group 2 bridges, where the initiation stage plays a more important role than for Group 1. Both the direct damage observations and the model predictions suggest that damage in Group 2 bridges will continue developing in the future at a slower rate than, but in comparable fashion to that observed in Group 1. It is cautioned

that other bridges in the inventory of ECR FDOT bridges have substructure with intermediate concrete permeability as in Group 2, so corrosion there may well begin to develop in the relatively near future. Speculative model projections for sound concrete locations in Group 3 and Group 4 bridges indicate that widespread damage from ECR corrosion is not expected for several decades into the future. Modeling from a companion investigation (FDOT Project BD544-31) suggests some incidence of spalling may also result if crack orientation with respect to the rebar was adverse and chloride transport into the crack was greatly enhanced with respect to the bulk. Additional data on the development of that localized corrosion at the Howard Frankland bridge will be necessary to implement an adequate modeling approach for those cases.

Electrochemical Impedance Spectroscopy (EIS) measurements of ECR in extracted cores showed good potential for non destructive characterization of the extent of coating damage. A possible method for accounting for frequency dispersion effects in the high frequency response (of importance to assess extent of defects) was introduced.

TABLE OF CONTENTS

ACKNOWLEDGEMENT

The assistance with field inspections of many collaborators at the FDOT State Materials Office and from Concorr Florida, Inc. is greatly acknowledged, as is that of numerous student participants in the University of South Florida College Of Engineering Research Experience for Undergraduates program and staff from the USF Nanomaterials and Nanomanufacturing Research Center. The assistance of Mr. Ivan Lasa of the FDOT State Materials Office in providing corrosion condition information for the Group 1 bridges is particularly acknowledged.

1 INTRODUCTION

Note: The technical content of this investigation is closely supplemented by that of the companion FDOT project, "Corrosion of Steel in Locally Deficient Concrete", BD544-31. To best use available resources, field surveys and related analysis were conducted concurrently for both projects. For contractual reporting purposes the findings under both projects are reported in separate documents. However, for technical discussion and elaboration of conclusions it has been often necessary to refer to and reproduce here some of the material from the Final Report for Project BD544-31, cited accordingly. It is recommended that both documents be consulted for an integral view of the issues concerned.

1.1 Project Scope

Epoxy coated steel reinforcement (ECR) was used for corrosion control in approximately 300 Florida Dept. of Transportation (FDOT) marine reinforced concrete bridges from the late 1970's up to the early 1990's. The use of ECR for new FDOT structures was discontinued upon mounting evidence of severe corrosion in some of the existing bridges.

Earlier investigations completed in 1993 assessed the corrosion condition of 20 FDOT ECR bridges after ~5-12 years of service [1]. A model of the corrosion mechanism of ECR in marine concrete was developed [2]. The corrosion was viewed as resulting from the presence of coating production imperfections (within allowable limits at the time of construction) then aggravated by fabrication, handling, and a severe construction yard environment which promoted coating-metal disbondment [3-5]. Disbondment was found to become more extended after only a few years of service in the marine structures. Early penetration of chloride ions to the rebar level resulted in severe undercoating corrosion, aggravated by extended macrocell formation with cathodes elsewhere in the rebar assembly [6-7]. Durability prognosis evaluations were formulated based on the research findings and application of an initiation-propagation deterioration model [1,4,8]. The structures showing early corrosion had been found to have concrete with high permeability. Based on measured concrete properties indicative of permeability, mainly the chloride ion diffusivity , the model projected development of corrosion after about one more decade of service (that is, at the beginning of this investigation) in some additional FDOT ECR structures with moderate permeability. The projections indicated a lesser likelihood of observing corrosion at that in other bridges with lower concrete permeability.

This investigation examined the present corrosion condition of those structures to validate and refine projections. Attention was given also to the possible effect of thin structural cracks on early corrosion in low permeability concrete [9]. Those cracks are usually <0.3 mm wide and typically one or more

meters of waterline perimeter apart, but significant preferential chloride penetration through those cracks has been noted at low elevations where the concrete is wet. As indicated above, this issue is closely supplemented by the work under the companion FDOT project BD544-31 and cross reference to the corresponding Final Report [10] will be made throughout this document.

1.2 Objectives

Per the scope stated above the objectives of this work were to:

1) Assess the present condition of ECR in the substructure of major FDOT marine bridges built starting about three decades ago, with attention to early warnings of corrosion damage development in structures not showing corrosion in the previous surveys.

2) Obtain information on the rate of penetration of chloride and other aggressive action in those bridges, and use that information together with that on present and past rebar condition to validate and improve predictive corrosion performance models.

3) Apply the improved models to project corrosion damage and repair needs over the remaining service life of those bridges, toward evolving recommendations for future maintenance strategies.

1.3 Approach

The following Tasks were addressed keyed to the above objectives:

Task 1. Assess present ECR condition. 18 ECR marine bridges (Table 1) were assessed. Bridges were selected to be representative of the following categories:

a) Group 1: Structures with documented severe early ECR corrosion during the 1991-93 investigation , to determine the progression of damage having already a well established baseline.

b) Group 2: Bridges not showing ECR corrosion in 1991-3 but determined to have a high likelihood of ECR corrosion development during the following decade based on high chloride ion diffusivity.

c) Group 3: Bridges with overall low to very low chloride diffusivity but where some narrow cracks have been detected that permit fast localized chloride ingress.

d) Group 4: Bridges with intermediate chloride diffusivity with some chances of ECR corrosion development at present.

Special bridge surveying and concrete/ECR core sampling were conducted for 13 structures from Groups 2-4. The surveys included visual examination of all or part of the substructure and soundings to assess extent of corrosion spalls if any was present. The present condition of Group 1 structures was determined based on routine FDOT inspections.

Task 2. Testing and Model Development. Field extracted cores were analyzed for penetration rate of chloride and other relevant aggressive action. Rebar condition as assessed in Task 1 and bridge spall records were correlated with bridge age and aggressive agent penetration to obtain functional relationships in the form of damage functions, using and expanding methodology already applied to several Keys bridges [2]. Electrochemical impedance were conducted with bridge extracted ECR to further characterize corrosion development. The tests sought to evaluate corrosion rate and extent of disbondment. The data obtained and analyzed under this task are used to formulate an advanced predictive model for damage progression in marine bridges using ECR. The model is based on the distributed corrosion model developed previously by the P.I. [8] where the substructure is divided into elements each with its own corrosion initiation-propagation parameters, and where the rebar diameter/cover ratio is an additional input parameter. The effect of cracked concrete is considered as well.

Task 3. Model Application for Prognosis and Future Strategies. The model developed under Task 2 was applied to the structures examined and to generic representatives of the existing FDOT inventory of bridges using ECR. Quantitative damage function projections in the form of future spall development were prepared for those structures and used to evaluate future repair/rehabilitation needs. The projected damage functions were calibrated as needed based on the already observed experience base for FDOT ECR bridges.

1.4 Bridges Investigated

Table 1 lists the structures of all groups, construction information, and the bridge identifications used in the rest of the report. 7MI, NIL and INK were built with drilled shafts supporting columns with connecting struts. The LOK bridge has capped drilled shafts joined by a strut, and V-Piers rested on synthetic rubber pads placed on the caps. The CH5 bridge has drilled shafts with spread footers and precast, posttensioned box columns. The CH2, VAC, and SNK bridges have capped drilled shafts supporting columns. The CHO bridge has reinforced concrete columns with connecting struts, supported by capped prestressed piles. The SSK substructure consists of reinforced concrete columns with footers and struts in the low approach spans and elliptical posttensioned columns for the high approaches. The PER substructure consists of reinforced concrete piles for the low approach and reinforced concrete columns on footers for the main span. The HFB substructure consists of reinforced concrete columns on footers.

Substructure in marine service for NWR, ITA, and ITB include the bascule and rest piers. IT2 and IT3 consist of reinforced concrete columns with footers. The substructure on these bridges was painted with a texture coating above the high tide level.

The concrete used in the substructure of Group 1 and 2 bridges was cast in place (CIP) and conforming to FDOT Class IV specifications at the time of construction. Those specifications established water-to cement ratio w/c<0.41, cement content = 388 kg/m3, and 28-day strength >23.5 MPa. The specified maximum chloride content (acid soluble test) for concrete in these structures was 0.24 kg/m^3. Group 3 bridges utilized advanced concrete mix designs that included pozzolanic cement replacement. Specifications for SSK included w/c<0.41, cementitious content 444 kg/m^3 including 20% Type F fly ash, and 28-day strength >34.5 MPa for non-mass concrete and w/c<0.35, cementitious content 388 kg/m^3 including 28.5% fly ash and 28-day strength >34.5 MPa. Specifications for the other two Group 3 bridges had lower cementitious content. HFB concrete mix specifications included w/c<0.41, cementitious content 388 kg/m3 including 35% Type C fly ash, and 28-day strength >34.5 MPa . ITA and ITB (Sunrise Blvd) were side by side twin bridges. ITB incorporated flyash and had much lower permeability than ITA. ITA is categorized with Group 4 Bridges and ITB is categorized with Group 3 Bridges. Further details on Group 2 bridge construction and durability issues is found in Reference [9].

2 INVESTIGATION METHODOLOGY

2.1 Bridge Survey

Representative locations from several substructure component types (columns, footers, struts) were selected for examination, focusing on cracks on concrete sections at low elevations exposed to sea splash. For SSK, higher elevation locations (~7-8 m above high tide) where wide cracks were observed were also examined. Elevations are reported as distance above the high tide level (AHT). The ECR segments (typically ~2 cm diameter, ~10 cm length) were perpendicular to the core axis. Concrete clear cover was noted and checks for concrete delamination were made by hammer sounding. When cracks were observed, pairs of cores were collected unless otherwise indicated along the same elevation typically ~15 cm apart on center with one core centered on crack. The in-situ condition of the exposed ECR coating was noted. Spot knife tests for coating disbondment were conducted. Electrical continuity between coring-exposed ECR segments was tested when possible to determine possible sources of corrosion macrocell phenomena. Half-cell potentials were measured with a copper/copper-sulfate reference electrode (CSE) along the elevation of the substructure component. Concrete surface resistance was measured using a Wenner array probe with an inter-probe spacing of 5 cm, chosen as a compromise between sampling size and possible interference from embedded rebar. Concrete porosity was measured following ASTM C642-97. ECR was extracted and examined. Autopsy of the coating was conducted for evidence of coating breaks, disbondment, backside contamination, and corrosion under the epoxy coating.

2.2 Chloride and Carbonation Penetration

Chloride ion penetration profiles were obtained for the field-extracted concrete cores. Powdered concrete samples obtained at various depths from the surface were analyzed for total (acid-soluble) chloride concentration; results are given in mg of Cl^- ion per gram of dry concrete. Diffusion coefficients, D, were estimated by least-error-fitting of the chloride content data to a solution to Fick's second law that assumes constant D and constant surface chloride concentration. Additional chloride penetration assessment and further details are detailed in the Report for BD544-31 [10].

The depth of concrete carbonation (from the external surface) was measured by lightly spraying 1% phenolphthalein in ethanol solution on freshly fractured concrete core samples. In concrete cores from cracked locations, the core was separated exposing the cracked surface, and phenolphthalein was sprayed on it. The depth (if any) from the external surface to which the crack surface remained colorless was recorded as the on-crack carbonation depth.

2.3 ECR Sample Characterization

The coating thickness was measured with a magnetic coating thickness gage. Visible coating defect areas were recorded and correlated to the ECR surface corrosion appearance.

To quantify coating disbondment, the coating adhesion strength was measured with a mechanical pull-off device [5]. A metal dolly (4.8 or 6.4 mm diameter) contoured to the surface curvature of bar between deformation ribs was attached with a cyanoacrylate adhesive to the outer polymer surface (lightly roughened and degreased) directly adjacent to the defect location. The polymer coating on the perimeter of the dolly was removed with a rotating dental drill bit. The dolly was then pulled until separation using a gimbal joint fixture to avoid shear stresses. The strength was recorded as the pull-off force divided by the nominal dolly area.

In the case of one of the bridges where deep localized surface corrosion was observed, metallographic micrographs of the apparent pit cross-section were prepared. The samples were prepared by normal metallographic grinding and polishing procedures (final polish with 0.05 μm alumina suspension) and etched with a 2% nitric acid in ethanol (nital) mix. Supplemental scanning electron microscopy and elemental analysis were conducted. A summary of important findings is given here with additional details reported in the Report for BD544-31 [10].

2.4 Electrochemical Impedance Spectroscopy

Pre-autopsy electrochemical impedance spectroscopy (EIS) measurements were made in the laboratory on the embedded ECR at the open circuit potential within 10 days of original extraction from the field (Figure 1). These tests were performed only in the large set of samples extracted from SSK, including cores extracted at both high and low elevations. On the cross-sectional cuts of the rebar, the circumference of the metal/epoxy interface was ground down and coated with acrylic (except at measurement contact point) to ensure electrical isolation of the steel substrate from the concrete matrix from the external surface of the sample. The signal amplitude was 10 mV and test frequency typically ranged from 100 kHz to 1 mHz. An activated titanium mesh at the core outer end face was used as a counter electrode and a short activated titanium wire (calibrated against a copper/copper-sulfate electrode, CSE) was used as a reference electrode held at the same end face. Both electrodes were separated and held by sponges saturated with tap water.

3 FIELD INVESTIGATION RESULTS AND DISCUSSION

Note: Examination of the bridges surveyed in this investigation was concurrent with field activities conducted under FDOT contract BD544-31. As such, bridge group nomenclature will be kept consistent with that in the companion report [10], from which portions are reproduced in the following for completeness and clarity. The organization of the material in the present report is different from that in [10], in that here chloride penetration and ECR condition are discussed jointly, as the latter is central to the objective of the present project. This Note also applies to subsequent Sections of this Report as to reproduction of excerpts from [9] as needed for completeness and clarity.

3.1 Field Survey and Sample Analysis Results

Detailed schematic representations of substructure elements of each bridge investigated, crack locations, and extracted core locations are given in Report BD544-31 Appendix I [10] and should be consulted for completeness.

3.1.a Group 1 Bridges (Severe Early Corrosion)

The following is a brief description of corrosion observations for this group [1] with updated results. Typical spalls (Fig. 2) affected a projected area of ~0.3 m^2 on the surface of the concrete. Longitudinal cuts on the ECR surface with a sharp knife permitted easy peeling of the coating from the corroded regions, revealing extensive solid dark undercoating corrosion products typically magnetic and electronically conductive [11]. Occasionally, significant amounts of acidic liquid rich in chloride and iron were found as well [3,6]. Coating disbondment was also found on rebar locations adjacent and away from corroding regions. This disbondment without significant corrosion was found to be widespread in ECR after it was in service for a few years in Florida marine substructure conditions of all this and the other groups, even in the absence of chloride contamination of the concrete next to the rebar [1,5]. Examination of the underside of coatings from numerous ECR samples from all bridge groups, did not reveal any correlation between this disbondment and the usual forms of surface contamination expected in the coating process [1,5]. Concrete resistivity readings as low as ~1 kΩ–cm in the tidal region indicative of high chloride diffusivities [1,12,13].

Chloride ion profiles indicated that extensive chloride penetration of the concrete had taken place in the splash zone of Group 1 structures (e.g., in the order of 4 kg/m^3 at rebar depths after only 2 yrs). Apparent chloride diffusion coefficients (D_{app}) determined from the chloride profiles for the splash zone ranged from ~10^{-8} cm^2/sec to as much as ~$6x10^{-7}$ cm^2/sec [1,14]

The updated damage function for the most current bridge surveys is shown in Figure 3. As will be detailed in Section 5, corrosion propagation continued to increase at a similar rate observed earlier.

3.1.b Group 2 Bridges (High D_{Cl}- Bridges)

Vaca Cut(VA1/2) and Snake Creek (SNK). For simplicity, the side-by-side bridges VA1 and VA2 are treated as one bridge in the following[1] unless indicated otherwise. The substructure from VA1/2 and SNK has only reinforced concrete drilled shafts in contact with the seawater. Concrete deterioration was generally inconspicuous with the exception of vertical cracks (0.08-0.3 mm wide) on one shaft each in VA1 and VA2 and one in VA1/2 and one in SNK, out of a combined total of 26 shafts in water for those bridges. The drilled shaft containing the largest crack in VA1/2 (0.3 mm width (Figure 4), 70 cm AHT, ~13 cm deep had also internal cracks (diagonal and transverse), leading from reinforcement depth, that had not yet propagated to the concrete surface. The crack at SNK was 0.08 mm thick, ~30 cm high from 4 cm below high tide line to 26 cm AHT, and ~18 cm deep. The reexamined drilled shafts did not have any discernable deterioration. Concrete delamination could not be detected by hammer sounding on the any of the concrete sections (sound or cracked) from either bridge likely due to the large concrete cover (~13-15 cm).

In VA1, two shafts were cored in five locations fully exposing ECR in three cores. Two of those cores were an on-crack and off-crack pair at the largest vertical crack, 46 cm AHT. The ECR, both on- and off- the main crack showed extensive corrosion (Figure 6a). Lesser but still significant corrosion distress was observed on samples from a core at 165 cm AHT. There, the distress was limited to small coating breaks of rusty appearance and to thin rust spots and discoloration on as much as 10% of the steel substrate observed after removal of the coating. ECR was fully exposed at four core locations in SNK, including a low elevation on- and off-crack pair that showed significant corrosion but not as severe as in VA1/2. Complete coating disbondment was observed on all ECR samples from both bridges. Where it could be examined, backside contamination was ~<1%. The average epoxy coating thickness was ~0.2 mm (Figure 5), generally consistent with product specifications. Vertical and horizontal ECR exposed by coring in the same column were mostly found to be electrically continuous. Half-cell potential mapping of the ECR (Figure 7a) generally showed potential values (more negative than -300mV CSE), traditionally indicative of corrosion activity for plain rebar in atmospherically exposed concrete. Although potential may not be a reliable indicator of active corrosion of ECR in marine concrete, it is noted that all the rebar which had showed visual signs of corrosion were similarly negative. Concrete resistivity (Figure 8a) reached <5 kΩ-cm, indicative of highly permeable concrete. A general trend of lower resistivity at low elevations was consistent with

[1] This follows a recent FDOT change in numbering to designate bridges 900124 (VA1, Southbound) and 900126 (VA2, Northbound) under the single number 900126.

expectations of near water saturation there. The large aggregate consisted of limestone. The volumetric porosity of the concrete from both bridges was high (~20%), consistent with the high permeability observed.

The chloride penetration profiles are shown in Figure 9a. The D values for VA1/2 were very high ($1x10^{-7}$ to $2.76x10^{-7}$ cm^2/s) and less but still indicative of high permeability for SNK ($4.73x10^{-8}$ cm^2/s). The average Cs value was similar to those measured in other Florida marine bridges (~7 mg/g, ~17 kg/m^3) [9]. The chloride content of the cracked concrete samples were higher than in the sound concrete within the area of the drilled shaft susceptible to sea splash (<46 cm AHT) which gives indication of preferential chloride penetration through the cracks.

William Marler (CHO). Two of 20 footers from the ten high elevation piers had cracks wider than 1.0 mm; ten of the footers had cracks larger than 0.2 mm. Minor concrete cracking was typical on all of the footers. Vertical and map-type cracking was observed on one of 20 columns from the high elevation piers. Rust bleedout was observed on two columns and one strut. The origin of that bleedout was not confirmed as samples of reinforcement were not obtained, but corrosion of reinforcement may be possible. Core samples were extracted from two footers each with one wide vertical crack (1.0 and 0.63 mm wide respectively). Approximately 0.42 m^2 and 0.1 m^2, respectively, of concrete around the crack locations seemed to be delaminated as determined by hammer sounding. Extensive corrosion of the reinforcing steel (Figure 6b) was observed on both footers at elevations 8.9 to 17.8 cm above high tide level, both where the crack intersected steel and in adjacent sound concrete locations. Lack of coating adhesion to the steel substrate was observed for all extracted ECR. The concrete cover to vertical bar ranged from 7.1-10.4 cm; nominal design cover was 10.2 cm. Highly negative half-cell steel potentials were measured, -400 to -552 mV CSE. In plain steel rebar such potentials would likely be reflective of the observed ongoing corrosion, but it is cautioned that potential readings in epoxy coated rebar, especially in wet concrete, may not be always reliable indicators of corrosion condition. Concrete surface resistivity measurements on the columns ranged from 46 to 128 kΩ-cm on the columns at elevations 0.6 to 2.4 m AHT. Concrete resistivity on the footer ranged from 16 to 63 kΩ-cm at elevations 0 to 0.55 m AHT. The large aggregate consisted of river rock. The volumetric porosity of the concrete was ~14%. All seven ECR samples from this bridge (sound and cracked concrete locations) showed significant loss of coating adhesion and severe corrosion of the steel bar.

Preferential chloride ion penetration through cracks in this bridge (similar to the other Category 2 bridges, Figure 9) was overshadowed by fast bulk diffusion through the sound concrete at low elevation locations exposed to sea splash. Chloride concentrations at reinforcement depths (10.2 cm)) for sound and cracked concrete locations were larger than the commonly assumed 0.7 kg/m^3 conservative chloride ion threshold value. The average chloride ion diffusivity for

sound concrete from this bridge was lower than that measured in an earlier investigation [1] but it was within the range of calculated diffusivities from the same investigation. Nevertheless, a high value was still calculated ($1.8x10^{-8}$ cm^2/s). On the crack plane, carbonation penetration depth was less than 1cm but otherwise negligible through bulk concrete.

Channel 2 (CH2). Corrosion evaluations at CH2 for the current investigation were cursory but those and records [15] from FDOT routine surveys showed extensive corrosion damage not unlike that observed at the Group 1 bridges (Figure 10). Typical corrosion distress is characterized by extensive concrete cracking (as wide as 1.3 mm with spalled concrete (average ~2.9 m^2) typically in the splash area but with several instances extended to above and below it. As in the Group 1 bridges, the concrete in CH2 showed indications of high permeability. At 25 y age the chloride concentration at ~15 cm reinforcement depth and elevations 0.3-2 m AHT was as much as 6.5 kg/m3. Assuming a typical chloride surface concentration value [9] Cs~20 kg/m^3, D_{app} was estimated to be in the order of ~10^{-7} cm^2/s. Low concrete resistivity (3-30 kΩ-cm) was measured as well at elevations 0.3-1.5 m AHT. Severe coating distress and disbondment was observed at spalled concrete locations. ECR in areas away from distressed concrete locations was not tested.

3.1.c Group 3 Bridges (Low D_{Cl}- Bridges)

Sunshine Skyway (SSK). The low approach span substructure consists of 512 reinforced concrete columns with footers and struts exposed to direct sea splash, and 256 cap beams at ~7 m AHT. The high approaches have elliptical post-tensioned columns. The average clear cover of the outer mat steel ranged from 9-11 cm in the various substructural components.

At low elevations, hairline cracks (<0.03 mm) were commonly observed on the concrete footers (<60 cm AHT) and columns (<200 cm AHT). Larger vertical cracks (~0.3 mm, (Figure 4)) with efflorescence were found on the elliptical post-tensioned columns. No concrete delamination was observed or detected by hammer sounding on any cracked or sound sections. A total of 16 cores were extracted from these low elevation locations. In the field, no evidence of corrosion was observed on the surface of the ECR exposed by coring, except for vestigial rust at small coating breaks such as high points on ribs where the coating had been damaged during or before construction. That rust did not appear to reflect ongoing corrosion. Spot knife tests of outer mat ECR exposed at the bottom of the core but not extracted, as well as from extracted bar segments indicated disbondment, in agreement with the laboratory findings described below. Whenever vertical as well as horizontal bars were exposed by coring, mutual electrical continuity was observed. Half cell potentials (Figure 7b) ranged from values indicative of passive behavior to <- 600 mV. The more negative values were observed at some (but not all) of the lowest elevations. As mentioned above, the significance of these values is limited. The surface

resistivity of the concrete at elevations where the concrete was very wet (e.g. <=0.3 m AHT) (Figure 8b) ranged from (~15-150 kΩ-cm), consistent with the low permeability concrete used in this bridge. The large aggregate consisted of limestone. The volumetric porosity of the concrete was ~20%. Carbonation penetration into the surface of the concrete at elevations exposed to sea splash was typically negligible in sound concrete, and in cracked concrete including on either side of the crack deeper into the core.

The trestle cap beams, at elevations 7-8 m AHT, often had wider structural cracks (up to 0.6 mm, (Figure 4)), some with heavy efflorescence. No concrete delamination was observed or detected. Moisture was more prevalent at some of the cap beams which were exposed to runoff water at deck expansion joints. Isolated concrete spalls (apparently not corrosion related) in the same vicinity of the cracks were occasionally found in cap beams. A total of 10 cores were extracted from the cap beams. As in the lower elevations, minor to no corrosion was observed on the ECR exposed by coring except for vestigial rust at small coating breaks. Spot knife tests on outer mat ECR had generally shown coating disbondment (Figure 11) but with some locations with good coating adhesion. There was no indication of electrical continuity between the vertical bars exposed by coring. Potentials measured at exposed ECR locations ranged from -70 mV CSE > E >-490 mV CSE. The concrete surface resistivity was 70-300 kΩ-cm with no clear difference between sound and cracked locations. Carbonation depth in bulk concrete in sound and cracked locations was typically small, ~1-2 mm but in one sound concrete case reached ~5 mm. There is some evidence of deep on-crack carbonation depth at these higher elevations reflecting dryer conditions. The average epoxy coating thickness from outer mat ECR at all locations was ~0.2 mm (Figure 4), as expected from material specifications. Figure 11 is representative of the metal and coating underside appearance of samples with disbonded coating as described below.

In the low elevation samples the coating could be easily separated from the substrate on the entire specimen surface, indicating complete coating disbondment. Backside coating contamination was typically observed on 1-2% of the peeled coating. Consistent with field observations, vestigial rusting was observed on the steel substrate exposed by coating breaks. The steel surface exposed after removing the coating was mostly bright metal with some discolored zones around the coating breaks. No preferential corrosion or coating disbondment was observed at the ECR zone intersected by a crack, compared to the rest of the rebar segment. In the cap beam coring, complete coating disbondment was observed on seven of the ten ECR samples, while failure of the coating upon knife peeling was mostly cohesive on the remaining three samples. Backside coating contamination in the disbonded samples and presence of rust and discoloration were comparable to those noted in the low elevation samples. No correlation was found between the presence or position of the crack and the extent or location of rusting or coating disbondment in the ECR segments.

Little to no corrosion was observed at any examined on-water locations despite the presence of pre-existing structural cracks as wide as ~0.3 mm and with well manifested enhanced chloride penetration there at SSK (Figure 9b). At elevations exposed to sea splash, chloride ion concentration at reinforcement depth for cracked concrete was ~2 kg/m^3, close to or exceeding typically assumed threshold values [16].

Howard Frankland (HFB). Vertical cracks were frequently observed on the concrete footers; several large cracks were as wide as 1.0 mm. The trace of the crack observed on the top of the footers of the larger cracks was several feet deep. Cracks of this type had been documented in previous inspections and are likely due to differential curing in the bulk of the concrete. Subsequent coring revealed that cracking sometimes propagated past reinforcement depth (10.2 cm). Six pairs of on-crack/off-crack core samples were extracted at 9.7 to 47 cm AHT from 5 footers (in one of those footers, coring was done on two separate faces). Significant localized corrosion (morphology discussed later) was observed on 4 out of 7 on-crack bars extracted from 4 locations at 3 of the footers. In one instance where two bars were extracted from the same core, only the bar with deeper cover (11.6 cm, 1.6 cm deeper than the bar with lower cover) showed corrosion. No physical indication of corrosion was observed at any of the matching sound concrete locations. Concrete delamination was not detected at either sound or cracked locations. Coating disbondment was generally observed particularly on bar locations with corrosion development, but large sections of bars occasionally had good coating adhesion. Concrete clear cover to horizontal reinforcement was 10.9 to 11.7 cm, meeting nominal design requirements (10.2 cm). Half-cell potentials ranged from -200 to -690 mV CSE measured at elevations from tidal zone to 0.9 m AHT (Figure 7b). The more negative values were from locations where ECR corrosion took place. As noted above, caution is in order on generalizing the significance of this observation. Concrete surface resistivity was very high (MΩ-cm range) even in the tidal zone (Figure 8b). These high values are not likely due to concrete carbonation, since carbonated concrete depth was small (<1mm) as it is typically so in similar marine substructures [17]. The large aggregate consisted of granite. The volumetric porosity of the concrete was ~12%. High surface concrete resistivity may be due in part to low permeability of the large aggregate.

The corrosion observed on the four ECR samples extracted from cracked locations from this bridge merits note. The crack plane was usually perpendicular to the rebar. Corrosion products were generally observed around locations with coating defects, especially near the intersection of the crack plane with the rebar. Upon removal of the coating (which was found to be fully disbonded) the underlying surface was relatively dry, with dark corrosion product regions. Results from further exploration of this dark corrosion region is summarized later in the report and also detailed in the final Report for Project BD544-31 [10].

Distinct preferential chloride penetration at cracks was observed in this bridge (Figure 9b), similar to that noted for the SSK, at elevations exposed to sea

splash. Chloride ion concentration at the 10 cm reinforcement depth for cracked concrete was greater than commonly assumed conservative threshold values 0.7 kg/m^3). Much lower chloride levels were measured at bar depth in adjacent sound concrete, consistent with the low chloride bulk diffusivity ~7x10^{-9} cm^2/s determined for this low permeability concrete.

Lillian (PER): Very little concrete deterioration was observed. Thin hairline cracks were observed occasionally. The main span footer had larger cracks (~0.3 mm) with indication of efflorescence, some of which had been repaired earlier on by epoxy-injection. Concrete cores were extracted sampling on and off a crack location at 1.1 m AHT. Also cores were extracted from a column with no concrete deterioration at 0.9 and 1.2 m AHT. Concrete cover ranged from 10.4 to 13 cm. Half-cell potentials ranged from -183 to -656 mV CSE at tidal to 1.5 m AHT (Figure 7b). Concrete resistivity of the footer and column ranged from 113 to 275 kΩ-cm at 0.3-2 m AHT (Figure 8b). The large aggregate consisted of granite. The volumetric porosity of the concrete was ~14%. No corrosion or only vestigial signs of surface corrosion discoloration were observed on extracted ECR. Coating defects affecting as much as 10% of the bar surface were observed on ECR from sound concrete locations. No coating defects were detected on ECR from the cracked concrete location. Full coating disbondment was observed at sound and cracked concrete locations.

Chloride diffusivity values were very low (~3x10^{-9} cm^2/s) in agreement with earlier measurements [1]. Enhanced chloride penetration was not observed in the limited number of samples extracted (Figure 9b) but similar condition as that measured for the Sunshine Skyway may exist.

Sunrise Blvd (ITB): Like the other Group 4 bridges described in the next section, the substructure concrete had a paint coating extending down to the high tide level. Only minor concrete cracking, <0.2 mm (Figure 4 (combined with ITA)) was observed. A concrete core was extracted on a vertical crack at ~80cm AHT and another core extracted on sound concrete offset 15 cm on center but at an elevation 20 cm above the crack concrete location to avoid other concrete cracks. The crack propagated deep into the concrete past reinforcement depth, Xc~11cm. The half-cell potential ranged from -61 to -218 mV_{CSE} at tidal zone to 1.2 m AHT. Concrete resistivity ranged from ~9 to 180 kΩ-cm from the tidal zone to 1.2 m AHT. The large aggregate consisted of limestone and river rock. The volumetric porosity of the concrete was ~20%. No observation of corrosion was observed on the surface of ECR. The ECR in cracked concrete was found to be disbonded, but good adhesion was maintained for ECR in the sound concrete location.

The chloride diffusivity was 3.8x10^{-9} cm^2/s. Earlier measurements [1] were on average 5.1x10^{-9} cm^2/s. As with the other Group 3 bridges, chloride penetration was slow. The surface chloride concentration was only ~3 mg/g (~8 kg/m^3). Enhanced chloride penetration through cracks was moderate and may

have been somewhat mitigated by low surface chloride concentration reflecting presence of surface coating. The on-crack carbonation depth was significant and in one case extended beyond reinforcement depth; however, carbonation penetration through bulk concrete was negligible.

3.1.d Group 4 Bridges (Moderate D_{Cl}- Bridges)

Lehman Causeway (IT2/3): Very little concrete deterioration was observed, although pre-existing damage prior to application of surface texture paint may have been obscured. Concrete cracks (typically ~0.08mm wide) were thin yet penetrated deep into the concrete. The cracks were often traced across the width of the footers and penetrated past reinforcement depths (Xc~7-10 cm). Concrete cores were extracted sampling ECR on and off crack locations ~50-120 cm AHT. Half-cell potentials ranged from -41 to -627 mV_{CSE} at tidal level to 1.2m AHT (Figure 7b); low concrete resistivity was observed, 4 to 12 kΩ-cm at 0.1-1.2 m AHT (Figure 8b). The large aggregate consisted of limestone and river rock. The volumetric porosity of the concrete was ~20%.The coating was fully disbonded on all extracted ECR samples. Only vestigial surface corrosion at coating defects was observed but in some instances extended well beyond the coating defect area under the disbonded coating. Undercoating corrosion discoloration was observed for all sampled bars.

The average chloride diffusivity was $3.9x10^{-8}$ cm^2/s, consistent with that measured earlier [1]. The chloride surface concentration was however low (0.7 mg/g (~2 kg/m^3)), approximately ten times lower than that typically encountered in the tidal region in similar environments in other bridges. As in Group 2 bridges, any enhanced transport through cracks was likely overshadowed by fast bulk diffusion. Carbonation depth on sound concrete was negligible. However, the on-crack carbonation depth was ~4cm.

S. Andrews Ave (NWR.: Only the bascule rest pier was accessible. There, no concrete deterioration was externally observed. However, surface paint may have masked pre-existing cracks as one thin vertical crack (0.05mm) was revealed after removing some of the paint. One core was extracted to sample the underlying bar there (~1 m AHT) and another core on sound concrete at an elevation ~40cm below (no side by side cores were extracted at this location). The crack was found to be very shallow, propagating only a few centimeters below the concrete surface. The half-cell potential of exposed ECR in the cracked concrete location was -400mV_{CSE}. Concrete surface resistivity was not measured as it would have necessitated removing the paint coating and damaged surface finish in a tourist attraction bridge. The large aggregate consisted of limestone and river rock. The volumetric porosity of the concrete was ~20%. Only vestigial surface corrosion of ECR at coating breaks was observed. The epoxy coating was found to be disbonded with bright, lustrous underlying steel.

The chloride diffusivity was 1.8×10^{-8} cm^2/s, consistent with earlier measurements [1]. As with IT2/3, chloride penetration was fast but with a low concentration profile. The surface chloride concentration was only ~0.2 mg/g (~0.5 kg/m^3). Any enhanced chloride penetration through cracks was likely overshadowed by fast bulk diffusion.

Sunrise Blvd. (ITA): Like the other bridges in Group 4, the substructure concrete had a paint coating extending down to the high tide level. Only minor concrete cracking, <0.2 mm (Figure 4 (combined with ITB)) was observed. A core was extracted from concrete with no deterioration ~62 cm AHT. The half-cell potential ranged from -200 to -370 mV_{CSE} at tidal zone to 1 m AHT. Concrete resistivity ranged from ~4 to 10 kΩ-cm from the tidal zone to 1 m AHT. The large aggregate consisted of limestone and river rock and the volumetric porosity of the concrete was ~20%, similar to ITB. No observation of corrosion was observed on the surface of ECR and was found to be disbonded.

The chloride diffusivity was 2.5×10^{-7}. Earlier measurements [1] were on average 2.6×10^{-8} cm^2/s. As with the other Group 4 bridges, chloride penetration was fast but at low concentrations. The surface chloride concentration was only ~0.2 mg/g (~0.5 kg/m^3). Any enhanced chloride penetration through cracks was likely overshadowed by bulk diffusion.

3.2 ECR Sample Characterization

3.2.a. Pull-off Strength Tests

Coating pull-off strength measurements supplemented field and laboratory knife test observations. It is noted that the pull-off tests were conducted on various spots of some of the ECR samples, and that large variations in strength values were noted in some cases from one part of the sample to another. Pull-off strengths for ECR from Group 2 Bridges ranged from low to negligible (Figure 12), in agreement with the observations of significant corrosion and extended coating disbondment reported above.

For ECR from Group 3 Bridges the coating pull-off tests gave results generally consistent with observations noted earlier ranging from instances of good coating adhesion to widespread coating disbondment. In high elevation SSK samples, where the coating had generally been found to have good coating adhesion, most of the pull-off strength tests resulted in the cyanoacrylate failing instead of the epoxy-steel substrate bond; indicating that its strength was above ~10 MN/m^2. In contrast, the coating failed at stresses as low as ~0.6 MN/m^2 in the low elevation samples, consistent with prevalent coating disbondment there as noted earlier. Coating failed at stresses below ~1 MN/m^2 on some of the HFB samples but the cyanoacrylate adhesive limit (~10 MN/m^2) was reached for the majority of the sample spots tested . Samples from PER, noted earlier to be disbonded, had also pull-off strengths that were as low as 0.6 MN/m^2.

The polymer coating on ECR from Group 4 Bridges had pull-off strength levels consistent with disbondment measurements as described above. Of note, samples from IT2/3 had among the lowest pull-off strengths.

3.2b EIS[2]

Figure 13 shows EIS results from disbonded and non-disbonded ECR samples from the high elevation trestle caps of SSK. The non-disbonded samples had an impedance response similar to that of an ideal capacitor, consistent with later direct examination that did not show visible coating breaks, . The curves from samples which were found to be disbonded, however, showed high frequency (hf) loops with diameters that varied by orders of magnitude. Similar hf loops were observed in side by side comparisons of EIS responses of ECR from cracked and non-cracked concrete from low elevations (all disbonded). As seen in Figure 14, the ECR from cracked locations generally had smaller hf loops than the ECR from the sound concrete. As expected and shown in the cumulative curves in Figure 15, the measured solution resistance was smaller at the low elevation locations as well as in cracked samples, where moisture content and water penetration is expected to be higher. The impedance modulus at low frequencies too was smaller for ECR from cores extracted from low elevations, which have higher water saturation (Figure 16).

The tested system can be idealized by a simplified analog of a coated metal with the presence of coating breaks (Figure 17), where Rs is the solution resistance, R_{po} is the coating pore resistance, Rp is the polarization resistance, and the capacitance of the coating and the interfacial capacitance of the steel are constant phase elements, CPE with admittance

$$1/Z_{CPE} = Y_o(j\omega)^n \qquad 1)$$

where Y_o is the pre-exponential admittance term, ω is the angular frequency, and n is a real number $0<n<1$. The analog of the impedance of ECR with no coating flaws may be further simplified as a plain capacitor with capacitance C_c

$$C_c = \varepsilon\, \varepsilon_0\, A/d \qquad 2)$$

where ε is the dielectric constant of the coating (~5), ε_o is the permittivity of free space (8.85×10^{-14} F/cm), A is the area of the metal coating (~20-50 cm^2) and d is the coating thickness (~0.2 mm). $C\sim10^{-12}$ to 10^{-11} F/cm.

The hf loop diameter corresponds to the combined coating pore resistance, R_{po}. Cumulative fraction curves of the pore resistance for all ECR measured with EIS (cracked/non-cracked concrete coatings) are shown in Figure 18. Smaller R_{po} values were generally observed at cracked concrete locations as

[2] Portions of this section are reproduced from Reference [18] which was prepared based on interim findings of this project.

seen also in Figure 14 for samples with direct on- and off- crack sample comparisons. The EIS response was found to be sensitive to moisture content especially in the presence of cracks. The differences of R_{po} values from cracked to non-cracked samples are likely indicative of larger electrolyte conductance to the steel at crack locations. Test artifacts may result from current leakage to the exposed steel on the sides of the core sample, uneven moisture distribution, and concrete drying after field extraction.

The coating CPE component showed sometimes strong frequency dispersion as manifested by n values as low as ~0.5 (Figures 19 and 20a). The dispersion likely reflects uneven current distribution due to cell geometry combined with high and uneven concrete resistivity. Such effect would be expected to be more noticeable in combination with higher surface admittances and indeed, smaller R_{po} values (typically from cracked concrete samples) were associated with low n values (Figure 19). There was only one instance where a low n value, <0.7, was observed from a sound concrete sample. Y_o varied widely (Figure 20b) but as seen in Figure 21, after normalizing for the coating thickness (d) and surface area (A), $\log(Y_o)$ showed clear correlation with the value of n. Extrapolation of that trend to n=1 yields a value $Y_o d/A \sim 4x10^{-13}$. Per Equation (2) that value corresponds to a coating dielectric constant $\varepsilon = (Y_o d/A)/(\varepsilon_0) \sim 5$, which is consistent with values typical for polymers. This plausible result suggests that a representation as in Figure 21 can serve to deconvolute the effect of obscuring artifacts from uneven current distribution. A detailed analysis of this issue will be presented in a future publication.

Faradaic processes are expected to dominate the low frequency impedance of steel exposed at the coating breaks and surrounding disbonded areas. The low frequency response in the Nyquist diagram shows a sloping line with values in the neighborhood of 45^o. This behavior may reflect a transmission line combination of current and interfacial capacitance under disbonded coating as noted previously for ECR systems [19].

Although test artifacts are present, EIS measurements may provide information on the presence of coating defects with possible implications for future non-destructive ECR investigations. The area of a coating defect (pore or coating break), $A'_{po,}$ is inversely proportional to the resistance of the defect, R'_{po}.

$$A'_{po} = k \times \rho / R'_{po} \qquad 3)$$

where k is a proportionality constant and ρ is the solution resistivity. The proportionality constant was determined by correlating the observed coating damage area with the pore resistance measured by EIS. For the sample population measured so far, k ~ 0.2. Figure 22 shows the comparisons for ECR samples where direct coating defect observations and impedance measurements could be made, indicating better than order-of-magnitude correlation (in cases where there were no observable coating breaks, a nominal detection area of 0.1

mm^2 was assumed). Figure 23 shows the cumulative fraction of the coating breaks as percentage of bar area either directly observed or estimated from impedance data when no direct observation autopsy was available. In the test samples, less than 2% damage was observed on ~10 cm segments, consistent with coating damage guidelines at the time of construction and subsequently updated.

3.2.c Metallographic Examination of HFB Corrosion Samples.

Exploration with a sharp knife tip at the dark corrosion region from HFB samples pried out some of the products, revealing pit-like features as shown in Figure 24. Sectioning of the bar with a thin diamond blade and water-free lubrication was performed at a pit-like location, with subsequent metallographic mounting of the section. The cross section (Figure 25) revealed that corrosion had affected a wide region, having proceeded in relatively uniform fashion within the region to as much as ~1 mm deep. Except for some surface reddening, the corrosion products in that region were dense and dark-gray, suggesting a low oxidation state. The corrosion product-base metal interface was examined at higher magnification revealing upon etching a ferrite-pearlite grain structure that extended, with no indication of microstructural alteration, all the way up to the corrosion penetration front where it was being consumed. Representative features are shown in Figure 26. This observation nearly rules out ascribing the observed features to causes alternative to corrosion, for example the presence of an isolated defect in the form of trapped slag or mill scale during rolling, since such condition would have been manifested by microstructural changes near the interface. Metallographic sections of the other bar samples from crack locations revealed corrosion penetration of depth and morphology similar to the one shown, always near the region of intersection of the rebar with the crack. Exposure of the metallographic sections to laboratory air resulted in slow reddening of initially dark products, as seen in Figure 25, suggesting that the corrosion product was evolving toward a higher iron oxidation state. No indications of severe corrosion were externally observed or revealed metallographically, on ECR from the peer cores on the sound concrete location next to the cracks.

4 CORROSION FORECAST MODELING

4.1 Corrosion Progression

The damage function trends shown in Figure 4 provide important insight on the extent of the corrosion of ECR in Florida bridges and its future development. For Group 1 Bridges the corrosion damage into the 3rd decade of service is extensive, with multiple spalls per pier on average. That damage affects a significant fraction of the area of the splash zone of each bridge, where the concrete surface area on the splash zone of a typical bent is ~ 20 m^2 and a typical spall affects ~0.3 m^2. Damage is likely to have been worse without the application of protective anodes in some of the structures. Except for an offset toward shorter times for NIL, the damage functions are remarkably similar to each other. The damage at present appears to increase approximately linearly with time. If those trends were to continue, the total extent of damage would roughly more than double over the next 20-30 years of service. As repairs in marine substructure are very costly, corrosion would place a continuing and heavy repair and maintenance burden during the remaining service life of these structures.

In Group 2 Bridges, corrosion propagation at CH2 started the earliest and appeared to increase roughly linearly with time similar to Group 1 bridges. Visible damage in the other Group 2 bridges appeared to have started after ~25 years in marine service. Corrosion deterioration was evident in CHO where spalled areas could easily be detected. Damage at VAC and SNK was not as conspicuous, and the concrete cracking at corroded bar locations there could not be established as resulting exclusively from expansive corrosion products; ie. some of the cracking may have been preexisting. The corrosion propagation trends at VAC and SNK may be anticipated to be similar to those at CH2 and the Group 1 bridges, but future confirmation is needed. In any event, the observation of significant ECR corrosion in the Group 2 Bridges verifies earlier damage projections for ECR structures in the Florida inventory having concrete with high D_{app} values [1].

For the Group 3 and 4 Bridges, no concrete delamination or spalling was observed at any of the structures examined, but significant ECR corrosion was observed at cracked concrete locations of HFB. This latter observation is an important warning of potentially severe local damage in the future, so frequent monitoring of these and similar locations are advisable. Due to the otherwise high quality concrete and large concrete cover, early corrosion damage is not anticipated for sound concrete locations. However, there was widespread disbondment of the epoxy coating in all these structures at low elevations even in sound concrete locations. This disbondment together with the frequently observed coating breaks is expected to facilitate corrosion initiation as chloride levels at the rebar depth increase in future decades.

4.2 Performance Projections[3]

To better understand the factors responsible for corrosion development and anticipate future needs for maintenance and repair, an effort was conducted to obtain quantitative damage projections. A statistical model to project performance of marine bridge substructure containing ECR was successfully applied in previous interpretations of the damage progression data [8]. Application to the current expanded data set is presented here. Briefly, the model divides the substructure surface into discrete elements, each experiencing damage evolution with a corrosion initiation stage (of duration ti) and a propagation stage of duration tp [12, 20] at the end of which the element is declared damaged. Each element is assumed to have its own value of surface chloride concentration C_s, concrete cover x, D_{app}, threshold concentration C_T. Those parameters together establish the local value of ti by assuming for simplicity a one-dimensional diffusion geometry [8]. The value of tp for each element is determined by assuming that the element has its own effective corrosion rate R resulting in corrosion penetration P that increases linearly with t-ti, where t is time. There is growing evidence that cracking/spalling takes place when P reaches a given value P_{CRIT} which for macroscopically uniform corrosion is proportional to the ratio x/ϕ, where ϕ is the rebar diameter [21]. Rebar size varies relatively little over the structural elements of interest (mostly near size #6 (diameter ~20mm) so by treating ϕ as constant tp may be approximated for modeling purposes [22] as tp = kx, where k is proportional to R^{-1}. R is strongly influenced by the condition of the coating [23, 24] such that ECR with substantial coating distress should corrode faster than in the absence of imperfections. Thus k is treated as a distributed model parameter that becomes smaller as the extent of ECR coating distress increases.

The values of Cs, D_{app} and x were assumed to have average values and element-to-element variability consistent with field observations in these structures. The variabilities were treated as stemming from normal distributions truncated as indicated below [8]. A fixed value of C_T was assumed for simplicity. Laboratory observations suggest that under simple conditions C_T for ECR is on the order of the value for plain steel bar [1], which may in turn be estimated as being proportional to the cement content (CF) of the concrete, $C_T \sim 0.004CF$ [16]. The parameter k was assigned variability but implemented only stepwise over 3 different finite levels, plus another level designating elements with essentially unblemished rebar coating. The fraction of elements having each of the coating distress levels (or lack thereof) was also a model input.

Damage projections were made by applying the above parameter distributions to a large population of elements, and tallying the fraction of elements reaching ti+tp for increasing time intervals [8]. Each element was

[3] Portions of this section are reproduced from Reference [25] which was prepared based on interim findings of this project.

assigned the same surface area value, equal to that of a typical spall, and the total number of elements corresponded to a multiple of the typical portion of a bent exposed to aggressive conditions. Thus the fraction of cracked/spalled elements at a given time was equal to the number of spalls per bent, allowing direct comparison to the field data.

Cases modeled corresponded to the Group 1 Bridges, and two subsets of the Group 2 bridges. Differentiation between cases applies only to x and D_{app} values. All calculations assumed initially chloride-free concrete.

Table 2 lists the values selected for model input for each case. The exposed bent area Af and element area Ae are based on typical prevalent structure and spall dimensions. The value of C_T reflects a representative value of CF (388 kg/m^3) consistent with those noted earlier. The average C_S, x and D_{app} values and their standard deviations are representative of those encountered in the affected bridges [1]. It is recognized that as those magnitudes cannot assume negative values, the actual distributions must depart from simple Gaussian shape. However, as more precise information on distribution character is not available, truncated normal distributions are used instead as a compromise. Thus all distributions are truncated at zero, and C_S is furthermore truncated at 25 kg/m^3 which is representative of a salt-saturated pore water condition [9]. The severe exposure regime and high concrete permeability conditions in Group 1 (reflected in the high average C_S and D_{app} values) result in exceeding the threshold concentration at the rebar depth very early (e.g one year or so) in the life of the structure even for average cover locations. Consequently, for Group 1 the corrosion development is expected to be dominated by the propagation stage (the value of tp), and less sensitive to the parameters that affect only ti [9].

The projected value of tp does depend strongly on x and k values. The first is measured directly, but the k distribution can only be inferred. Toward representing closely the observed damage progression, the assignment of k values over the rebar assembly was made by assuming that only a small fraction (2%) of the rebar assembly was responsible for the earliest observations of damage. That fraction had a low value of k =0.14 y/mm, which results in tp=7 years when x=50 mm. As ti is very short, that fraction was consequently responsible for the very first failures projected. Increasingly large fractions of the assembly were assumed to have correspondingly less distress and larger propagation times. This approach reflects the expectation that rebar segments with a high incidence of coating distress are likely to have the highest corrosion rates and therefore the shortest tp values. The chosen distribution for k then effectively states that there was a small fraction of the rebar with severe coating distress, and proportionally less distress on increasingly larger fractions of the assembly.

Resulting projections for each of the cases (thick solid line) are shown in Figures 27-28. The corresponding actual damage functions from Figure 3 are

reproduced for each pertinent case. The model projection for Group 1 bridges (Figure 27) reasonably reproduced the duration of the initial period where damage was minimal, and the subsequent steady rise. The present choice of input parameters replicates that used in Ref 8, which was based on fitting to data that terminated at earlier times for two of the bridges (NIL and LOK), but the overall match continues to be similarly adequate for the newer data as well. Sensitivity tests confirmed that the damage projection was only modestly influenced by changes in the distribution of D_{app} or Cs, or by variations in C_T, in agreement with the basis for the choice of model parameters indicated above. Additional calculations with alternative k distributions indicated also that reasonable fit to observed behavior could be obtained only if the percentage of the assembly assigned low k values (yielding tp values of only a few years) was quite small.

The dashed lines in Figures 27-28 represent the separate contribution to the total damage of each of the finite assumed distress fractions; addition of which corresponds to the thick solid line. As shown in Figure 27, as time progresses the projected damage increase results from fractions with increasingly greater k. Whether future damage will continue along the present trend depends, in this scheme, on the extent of coating distress on the rest of the rebar assembly. If the remaining rebar coating were in very good condition, damage would continue for some time at the present nearly constant rate and then saturate at some intermediate level. The present choice of k distribution assigns finite values to only the first 14% of the rebar assembly, so projected damage saturation would take place at ~9 spalls per bent. At present the highest recorded value (for NIL, evaluated in 2008)) reaches 4.4 spalls per bent without signs of slowing down, but the available data cannot preclude development of saturation in the relatively near future. Conversely, if the surface condition of the remaining rebar were poor or marginal, damage progression could easily continue to reach increasingly higher levels.

Data for the Group 2 bridges are too limited for detailed evaluation, but the model projections are in the order of the observed deterioration. Both subsets projected later damage development than for Group 1. The subset VA1/2, SNK, and CH2 (VSC on Table 2) had values of D_{app} that were comparable to each other but not much smaller than those for Group 1. However, the average rebar cover of subset VSC was twice as high as for Group 1. Under the model ruling equations [8] doubling the cover resulted in a fourfold increase in ti, and in doubling the value of tp which shifted the development of damage accordingly. The actual damage evolution in CH2 is somewhat faster than its projected value, but that difference partially stems from imprecise information on the range of D_{app} for that bridge as only a cursory examination performed there. CHO was placed into another subset (C on Table 2) as its average D_{app} was notably smaller than for the other bridges. That difference resulted in a significant increase of projected ti, toward increasing initiation stage control of the deterioration. Thus,

CHO had longer projected times to damage than in the first Group 2 subset, even though the average cover value was less than for that first subset.

The prevalent values of D_{app} for the sound concrete portions of the Group 3 bridges are approximately two and one orders of magnitude lower respectively than those in Groups 1 and 2. Therefore, model predictions for the 30-year interval used would have yielded essentially zero damage for the 30-year time interval covered in Figures 27-28. Damage projections for sound concrete in the Group 4 Bridges would be equally nil for that interval, not because of low chloride diffusivity but instead due to the low surface chloride concentration in that group.

Speculative projections for sound concrete in Groups 3 (lower substructure only) and 4 over a 100 year time frame are given in Figures 29-30. Those projections were made by assuming that the distributions of rebar damage and relative parameter variance and truncations were equal to those in Group 2, and changing only the average values of the concrete cover, chloride diffusivity, and surface concentration to reflect those obtained from concrete cores. A separate modeling case for Group 3 ITB (lower Cs) was not considered as damage would be expected to be lower here than at other Group 3 Bridges due to less chloride penetration. The projections are labeled speculative as there is no direct observations of damage to contrast against as it was the case for Groups 1 and 2. The projections essentially indicate that in sound concrete for Groups 3 and 4 widespread damage from ECR corrosion is not expected for several decades into the future. As noted above when considering similar expectations from earlier model predictions, much of the projected extended durability in these groups is a consequence of either high quality concrete or mild surface chloride load, and essentially no credit is taken for the use of ECR.

The model projections in this report do not include direct provisions for the effect of cracks on durability, as they are addressed in detail in the companion Final Report for Project BD544-31[10]. However, comments on the implications of cracking on durability are presented in the next section.

The interpretation and model described above involve numerous assumptions and simplifications. One such simplification includes assuming simple Fickian diffusion with time and depth independent D_{app} with constant surface concentration Cs.[8]. Notable among the many issues not addressed are alternative C_T regimes as reported elsewhere [14], including possible higher C_T due to coupling with nearby anodic regions [26] which could substantially alter the damage projection. This latter factor is examined in detail in Ref [27]. Future model improvements should resolve some of these issues. The present projections nevertheless serve to provide insight on the key factors responsible for the observed damage and in formulating corrosion management strategies.

4.3 Overall considerations and behavior in locally deficient concrete

The field observations and insight from the above modeling projections indicate that ECR corrosion in the Florida bridges resulted from a combination of factors. Those include a highly aggressive service environment which, in the absence of a thick cover of highly impermeable concrete, rapidly left the epoxy film as the only remaining corrosion protecting barrier on the steel bar. Given also the inherent vulnerability of the film to flaws and disbondment from the base metal, corrosion quickly ensued with electrochemical aggravating factors noted earlier. As the modeling arguments showed, significant corrosion of even a relatively small fraction of the rebar assembly could manifest itself as extensive and conspicuous damage, which can continue increasing for many years.

As shown by the absence of external signs of damage in the Group 3 bridges, no severe ECR corrosion developed when the coated bar was protected by a thick cover of sound, very low permeability concrete with D_{app} values nearly two orders of magnitude lower than those in Group 1. Significant amounts of coating flaws existed in those cases too, as well as widespread loss of adhesion between coating and base metal, so corrosion is expected to ensue once the chloride content at the rebar exceeds an effective threshold level. However, such event would likely be many decades into the future given the very slow chloride penetration. It is cautioned that part of the inventory of ECR Florida bridges has substructure with intermediate D_{app} values not unlike those in CHO [1]. In those bridges corrosion may well begin to develop in the relatively near future, albeit per experience from the Group 2 bridges and per model projections, at a more moderate rate of increase than that seen in Group 1.

As noted above and from findings in related investigations [1] the protection of a thick cover of low permeability concrete can be seriously diminished locally in the presence of cracks, lift lines or other local deficiencies. Corrosion may not only develop locally as noted in HFB, but the strong deterioration seen there may reflect also adverse galvanic coupling with nearby passive steel at other coating break locations [28, 29]. Such effect could lead to severe local reduction of cross section and associated risk of reinforcement failure [30]. The consequences of that form of deterioration may be mitigated in part by the relatively small incidence of cracking [9] when viewed in terms of number of cracks per length of waterline perimeter, thus representing a limited number of spots with likely incidence of damage. As shown in the companion report [10], also some incidence of spalling may result if the crack orientation with respect to the rebar was adverse and chloride transport into the crack was greatly enhanced with respect to the bulk. In addition to the continuing monitoring of these locations recommended above, further development of predictive models to cover this form of damage and quantify its effects should be conducted as well.

5 CONCLUSIONS

1. Damage from corrosion of ECR has continued to develop steadily in the substructure of the five major Florida Keys bridges (Group 1). Since the first indications of corrosion ~6 y after construction, damage increased at a rate of ~0.1 spall per bent per year until the present ~25 y age of the structures, with no indication of slowdown.

2. Externally recognizable ECR corrosion damage began to be noticeable at four other Florida bridges (Group 2) ~2 decades after construction and continuing into the 3rd decade. This observation confirms previous corrosion durability projections of early damage based on the high chloride diffusivity values prevalent in these bridges.

3. No severe ECR corrosion developed in situations where the coated bar was protected by a thick cover of sound, very low permeability concrete as encountered in Group 3 bridges. This confirmed previous modeling projections based on the very low chloride permeability of the sound concrete in these bridges. However, there was widespread disbondment of the epoxy coating in all these structures even in sound concrete locations. This disbondment together with observed frequent coating breaks are expected to facilitate corrosion initiation as chloride levels at the rebar depth increase in future decades.

4. Severe corrosion was also absent from locations in two of the Group 3 bridges where preexisting concrete cracks had allowed localized chloride ion penetration. However, in the other bridge in this group (Howard Frankland) significant ECR corrosion was observed at previously cracked concrete locations where the crack intersected the rebar.

5. The observation of ECR corrosion at cracked locations of a low permeability concrete bridge is an important warning of potentially severe local damage in the future. Frequent monitoring of these and similar locations is advisable, as is the development of predictive models for corrosion of ECR in locally deficient concrete.

6. A predictive ECR corrosion model was applied that replicated most of the damage function features observed in the field. The model divides the substructure in separate elements with individual chloride exposure, concrete permeability, concrete rebar cover, and extent of ECR coating imperfections.

7. Experimental results and predictive model calculations indicate that the propagation stage of corrosion dominated damage development in the structures that showed early deterioration (Group 1 bridges). Significant corrosion of even a relatively small fraction of the rebar assembly could

manifest itself as extensive and conspicuous damage, which can continue increasing for many years.

8. The model projections account for the observed later development of corrosion in Group 2 bridges, where the initiation stage plays a more important role than for Group 1. Both the direct damage observations and the model predictions suggest that damage in Group 2 bridges will continue developing in the future at a slower rate than, but in comparable fashion to that observed in Group 1. It is cautioned that other bridges in the inventory of ECR FDOT bridges have substructure with intermediate concrete permeability as in Group 2, so corrosion there may well begin to develop in the relatively near future.

9. Speculative model projections for sound concrete locations in Group 3 and Group 4 bridges indicate that widespread damage from ECR corrosion is not expected for several decades into the future. Modeling from a companion investigation (FDOT Project BD544-31) suggests some incidence of spalling may also result if crack orientation with respect to the rebar was adverse and chloride transport into the crack was greatly enhanced with respect to the bulk. Additional data on the development of that localized corrosion at the Howard Frankland bridge will be necessary to implement an adequate modeling approach for those cases.

10. Electrochemical Impedance Spectroscopy (EIS) measurements of ECR in extracted cores showed good potential for non destructive characterization of the extent of coating damage. A possible method for accounting for frequency dispersion effects in the high frequency response (of importance to assess extent of defects) was introduced.

6 REFERENCES

1. Sagüés, A.A. et al. “Corrosion of Epoxy Coated Rebar in Florida Bridges.” Final Report to Florida D.O.T. WPI 0510603. May 1994. Available online, www.dot.state.fl.us

2. Sagüés, A.A., R. Powers, and R. Kessler. Corrosion/2001. Paper No.06142. NACE International. Houston, TX. 2001.

3. Sagüés, A.A and R. Powers. Corrosion/1990. Paper No. 311. Nace International, Houston, TX. 1990.

4. Sagüés, A.A. Corrosion/1994. Paper No.299. NACE International. Houston TX,.1994.

5. Sagüés, A.A. and R. Powers. Corrosion/1996. Paper No.325. NACE International. Houston, TX. 1996.

6. Sagüés, A.A., H. Perez-Duran, and R. Powers. Corrosion. Vol.47, p.884. 1991.

7. T. Nguyen and J.W. Martin, JCT Research. Vol.1, no.2. pp.81-92. 2004.

8. Sagüés, A.A. Corrosion. Vol.59, p.854, 2003.

9. Sagüés, A.A. and S.C. Kranc, F. Presuel-Moreno, D. Rey, A. Torres-Acosta, L. Yao. “Corrosion Forecasting for 75-Year Durability Design of Reinforced Concrete.” Final Report to Florida D.O.T. WPI 0510805, Contract No. BA-502. December, 2001. Available online, www.dot.state.fl.us

10. Lau, K. and Sagüés, A.A., "Corrosion of Steel in Locally Deficient Concrete", Final Report to Florida D.O.T., Contract BD544-31, February 28, 2009. To be available online simultaneously with the present report, www.dot.state.fl.us

11. Sagüés, A., Powers, R., Zayed, A., "Marine Environment Corrosion of Epoxy-Coated Reinforcing Steel", in Corrosion of Reinforcement in Concrete, C. Page, K.Treadaway and P. Bamforth, Eds., pp.539-549, Elsevier Appl. Sci., London-New York, 1990.

12. Berke, N.S. and Hicks, M.C., "Estimating the Life Cycle of Reinforced Concrete Decks and Marine Piles using Laboratory Diffusion and Corrosion Data", p. 207 in Corrosion Forms and Control for Infrastructure, ASTM STP 1137, Victor Chaker, Ed., ASTM, Philadelphia, 1992.

13. Andrade, C., Alonso, C. and Goni, S., "Possibilities for Electrical Resistivity to Universally Characterise Mass Transport Processes in Concrete", p.1639, in Concrete 2000, Vol 2., R.K. Dhir and M.R. Jones, Eds., E. & F.N. Spon, London, 1993.

14. Hartt, W., Lee, S.K. and Costa, J., “Condition Assessment and Deterioration Rate Projection for Chloride Contaminated Concrete Structures” p.82 in Repair and Rehabilitation of Reinforced Concrete Structures: The State of the Art, W.P. Silva- Araya, O. T. de Rincon and L. Pumarada O'Neill, Eds., ASCE, Reston, VA, 1998.

15. Florida Department of Transportation Corrosion Research Laboratory. "Corrosion Condition Report. Florida Bridge Number 900097 Channel 2 Bridge". Jan. 21, 2005.

16. Bentur, A., Diamond, S. and Berke, N., Steel Corrosion in Concrete, E&FN Spon, New York, 1997.

17. Sagüés, A.A. E.I Moreno, W. Morris, and C. Andrade, “Carbonation in Concrete and Effect on Steel Corrosion,” Final Report to Florida D.O.T. WPI 051685, June 1997, Available online, www.dot.state.fl.us.

18. Lau, K. and Sagüés, A. A., "Coating Condition Evaluation of Epoxy-Coated Rebar", pp. 81-92, ECS Transactions Vol. 13, Issue 13, 210th ECS Meeting , October 29-November 3, 2006, Cancun, Mexico, "Corrosion of Infrastructure", The Electrochemical Society, Pennington, NJ, 2007.

19. Sagüés, A.A. and Zayed, A.M. *Corrosion*. Vol.47, p.852, 1991.

20. Tuutti, K., Corrosion of Steel in Concrete, Swedish Cem. and Conc. Res. Inst, 1982.

21. Torres-Acosta, A., Sagüés, A.A., ACI Mater. J. 101, 6 (2004): p. 501-507.

22. Torres-Acosta, A., Sagüés, A.A., “Concrete Cover Cracking with Localized Corrosion of the Reinforcing Steel”, p. 591 in Proc. of the Fifth CANMET/ACI Int. Conf. on Durability of Concrete, SP-192, V.M Malhotra, Ed., American Concrete Institute, Farmington Hills, Mich., U.S.A., 2000.

23. Clear, K.C., "Effectiveness of Epoxy-Coated Reinforcing Steel", Concrete International, p. 58, Vol. 14, May 1992.

24. McDonald, D.B, Pfeifer, D.W. and Sherman, M.R, "Corrosion Evaluation of Epoxy-Coated, Metallic-Clad and Solid Metallic Reinforcing Bars in

Concrete", Report No. FHWA-RD-98-153, Nat. Tech. Info. Service, Springfield, VA, 1998.

25. Sagüés, A.A., Lau, K, Powers, R.G. and Kessler, R.J. "Corrosion of Epoxy-Coated Rebar in Marine Bridges- a 30 Year Perspective", Paper No. 4039, Proceedings of the 17th International Corrosion Congress "Corrosion Control in the Service of Society", October 6-10, 2008, Las Vegas, Nevada, Published by NACE International, Houston, 2009

26. Sagüés, A.A. and Kranc, S.C. "Model for a Quantitative Corrosion Damage Function for Reinforced Concrete Marine Substructure" in Rehabilitation of Corrosion Damaged Infrastructure, p.268, Proceedings, Symposium 3, 3rd. NACE Latin-American Region Corrosion Congress, P.Castro, O.Troconis and C. Andrade, Eds., ISBN 970-92095-0-7, NACE International, Houston, 1998.

27. Sagüés, A.A., Kranc, S.C. and Lau, K. "Modeling of Corrosion of Steel in Concrete with Potential-Dependent Chloride Threshold", Paper No. 4006, Proceedings of the 17th International Corrosion Congress "Corrosion Control in the Service of Society", October 6-10, 2008, Las Vegas, Nevada, Published by NACE International, Houston, 2009

28. Kranc, S.C. and A.A. Sagüés "Computation of Corrosion Distribution Of Reinforcing Steel in Cracked Concrete", in Proc. International Conference on Corrosion and Rehabilitation of Reinforced Concrete Structures, Orlando, FL, Dec. 7-11, 1998, CD ROM Publication No. FHWA-SA-99-014, Federal Highway Administration, 1998.

29. Raupach, M. Construction and Building Materials, Vol. 10, p. 329, 1996.

30. Tinnea, J. "Localized Corrosion Failure of Steel Reinforcement in Concrete Field Examples of the Problem." 15th Int. Corr. Conference. Paper 706. NACE Int. Houston, TX. 2002.

Table 1. ECR Bridges

	Bridge Name			Year Built	Average D (cm^2/s)	ρ (kΩ-cm)	Cement factor (kg/m^3)	Fly ash	Widest crack width (mm)	ECR cover (cm)
Group 1	Seven Mile	7MI	900026	1982	$2x10^{-7}$	5-24	388	no	>1†	7.6
	Niles Channel	NIL	900117	1980	$2x10^{-7}$	-			>1†	
	Indian Key	INK	900095	1981	$\sim10^{-7}$	-			>1†	
	Channel 5	CH5	900098	1982	$\sim10^{-7}$	-			>1†	
	Long Key	LOK	900094	1982	$2.9x10^{-7}$	-			>1†	
Group 2	Channel 2	CH2	900097	1981	$\sim10^{-7}$	0.4-12	388	no	>1†	15.3
	Vaca Cut	VA1	900126	1982	$2.6x10^{-7}$	4-50			0.28	15.3
		VA2	900124	1982						
	Snake Creek	SNK	900077	1981	$9.0x10^{-8}$	4-50			0.28	15.3
	William Marler (over Choctawachee Bay)	CHO	570082	1979	$1.8x10^{-8}$	16-128			>1†	7.6
Group 3	Sunshine Skyway	SSK	150189	1986	$1.1x10^{-9}$	150	445	20% Type F	0.64	10.2
	Lillian (over Perdido Bay)	PER	480140	1981	$3.1x10^{-9}$	113-275	- *	Yes	0.25	10.2
	Howard Frankland	HFB	150210	1991	$7.3x10^{-9}$	high MΩ-cm	388	35% Type C	>1	10.2
	Sunrise Blvd. (over Intracoastal Waterway)	ITB	860467	1989	$3.8x10^{-9}$	9-180	-	Yes	0.18	12.0
Group 4	S. Andrews Ave. (over New River)	NWR	860319	1981	$1.8X10^{-8}$	-	-	no	hairline	11
	Sunrise Blvd. (over Intracoastal Waterway)	ITA	860466	1989	$2.5x10^{-7}$	4-10	-		0.18	10.9
	Lehman Cswy. (over Intracoastal Waterway)	IT2	870607	1983	$3.9x10^{-8}$	4-12	-		0.25	9.2
		IT3	870606	1983						

† Spalled Concrete, - data not available, * variations in concrete design for different substructural components.
For further details see Final Report of companion project BD544-31 [10].

Table 2. Damage Projection Model Input Parameters

		Group 1	Group 2		Group 3	Group 4
			(VSC)	(C)		
Af	Surface area of bent exposed to severe corrosion	20 m^2				
Ae	Typical spall area	0.3 m^2				
C_T	ECR chloride concentration threshold	1.55 kg/m^3				
μCs	Average surface chloride concentration	12 kg/m^3				6 kg/m^3
σCs	Standard deviation of surface chloride conc.	Cs/4				
Cs_{max}	Maximum surface chloride concentration	25 kg/m^3				
μx	Average rebar cover	76 mm	148 mm	87 mm	102 mm	
σx	Standard deviation of rebar cover	x/4				
μD_{app}	Average apparent chloride diffusion coefficient (m^2/s)	$2x10^{-11}$	$1.7x10^{-11}$	$1.3x10^{-12}$	$3x10^{-13}$	$3x10^{-12}$
σD_{app}	Standard deviation of app. diff. coeff.	D/4				
k'	Standard deviation of app. diff. coeff. proportionality constant for propagation time (Percentages indicate fraction of the surface assigned to the value).	0.14 yr/mm (2%);				
		0.28 yr/mm (4%);				
		0.56 yr/mm (8%).				

Note: Cs, x and D_{app} were assumed to be distributed as in an standard deviation, but truncated by zero and as shown by Cs_{max}, and normalized accordingly.

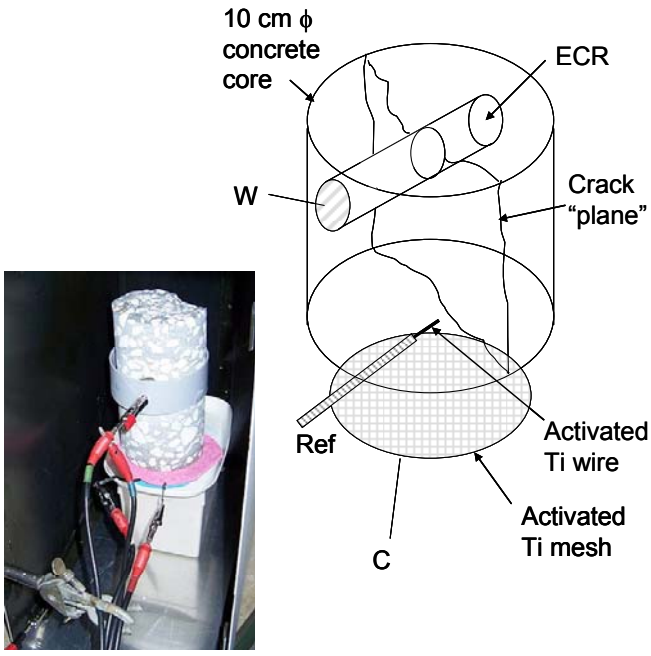

Figure 1. Field-Extracted ECR Concrete Core EIS Test Set-up.

Figure 2. Typical Spall Appearance (7MI). Figure from Ref [1].

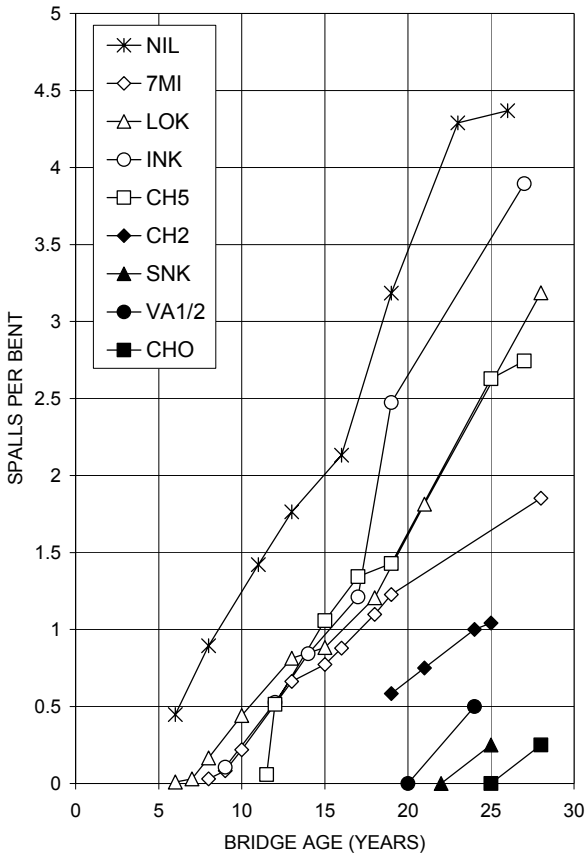

Figure 3. Progress of concrete corrosion damage as function of time.

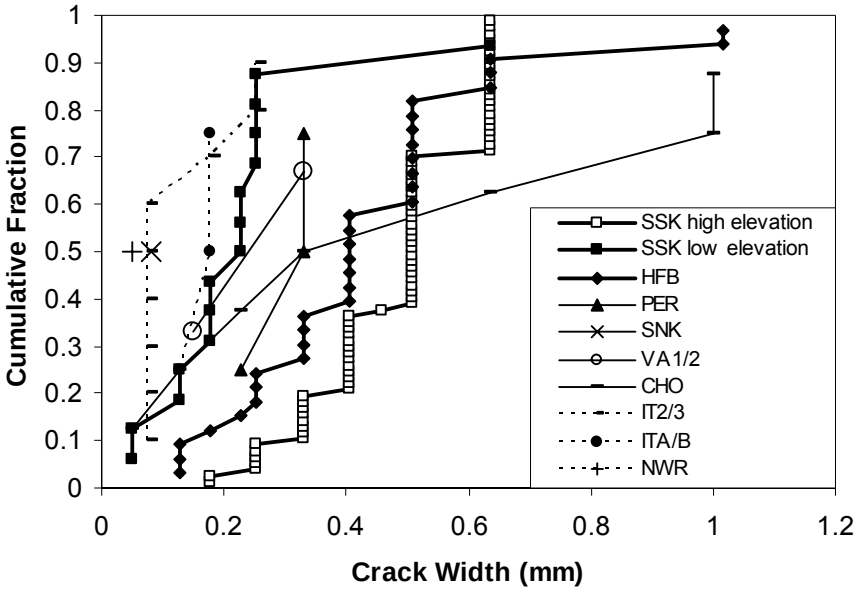

Figure 4. Widest crack width per substructure unit (*e.g.* per column, footer, *etc*.)

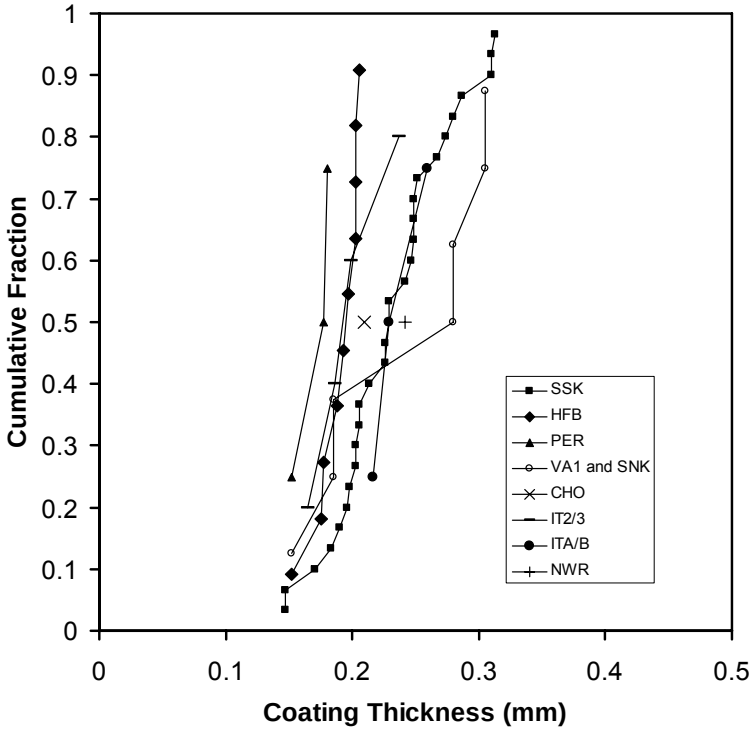

Figure 5. Epoxy coating thickness.

a) VA1 Drilled Shaft (VA2A2)~45 cm AHT on crack (0.33 mm).

b) CHO. Footer (CHO29S1). ~9 cm AHT.

Figure 6. Severe ECR corrosion in Group 2 bridges

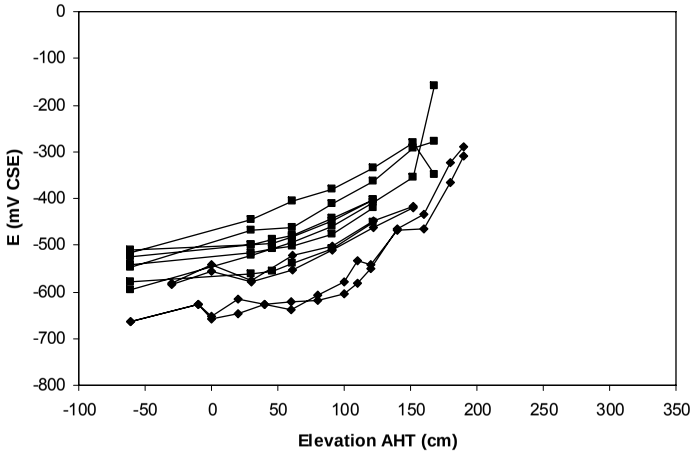

a) Group 2 Bridges. Square: VA1/2, Diamond: SNK

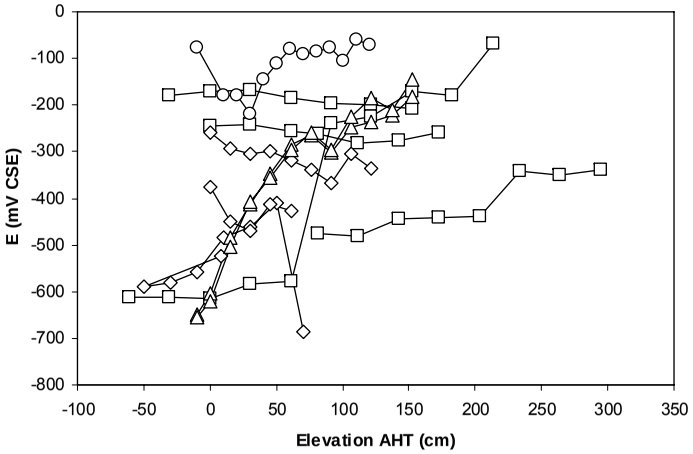

b) Group 3. Square: SSK, Diamond: HFB, Triangle: PER, Circle: ITB

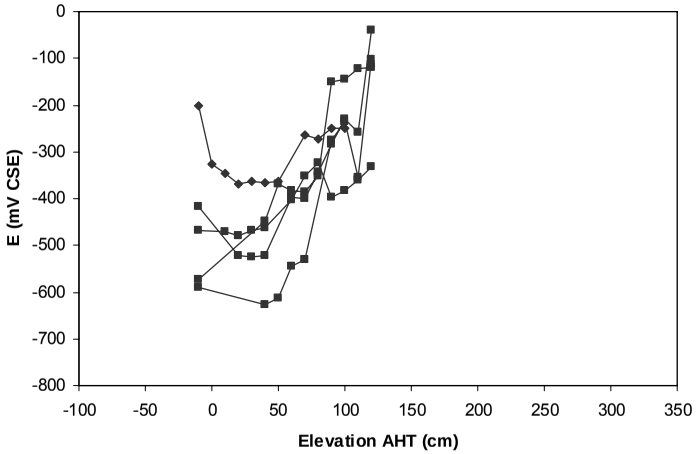

c) Group 4. Square: IT2/3, Diamond: ITA

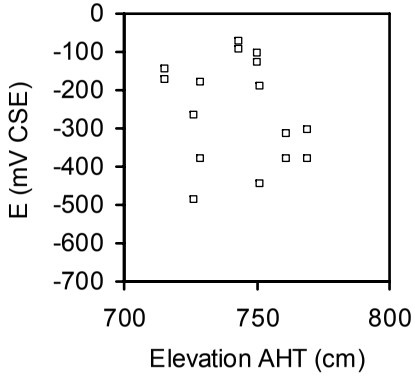

d) Group 3. SSK Trestle Cap Locations.

Figure 7. Open circuit potential evaluation as function of elevation.
Refer to the Appendix for numeric data listing.

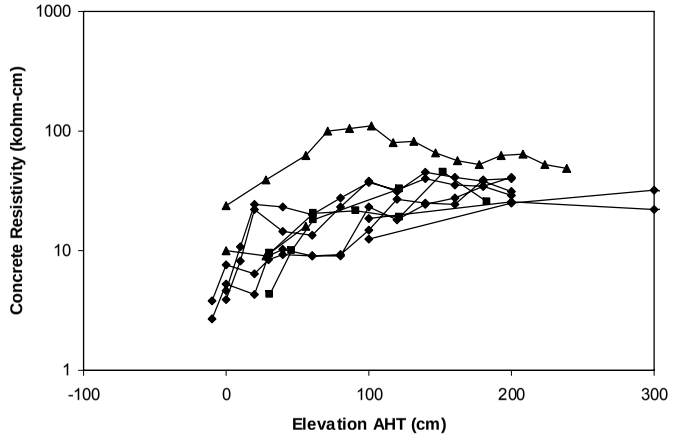

a) Group 2 Bridges. Square: VA1/2, Diamond: SNK, Triangle: CHO

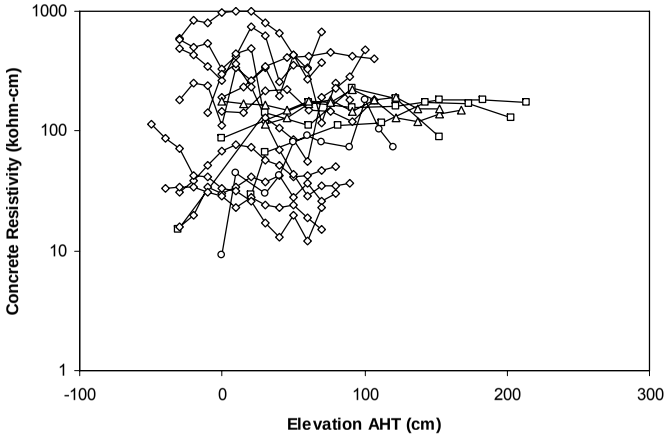

b) Group 3. Square:SSK, Diamond: HFB, Triangle: PER, Circle:ITB

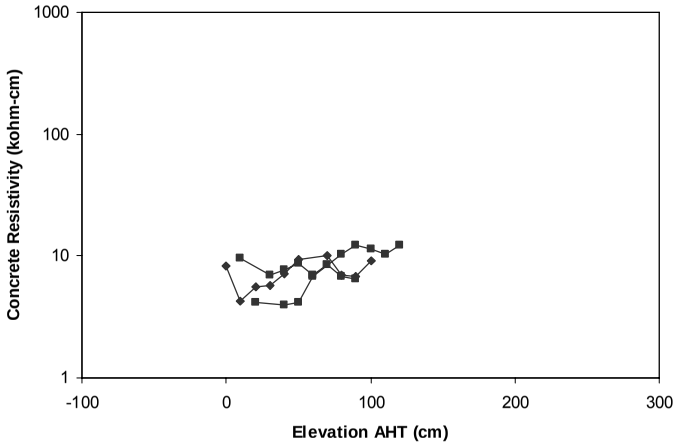

c) Group 4. Square: IT2/3, Diamond: ITA.

Figure 8. Concrete surface resistivity evaluation as function of elevation. Refer to Appendix II of Final Report of companion Project BD544-31 [10] for numeric data listing and detailed location.

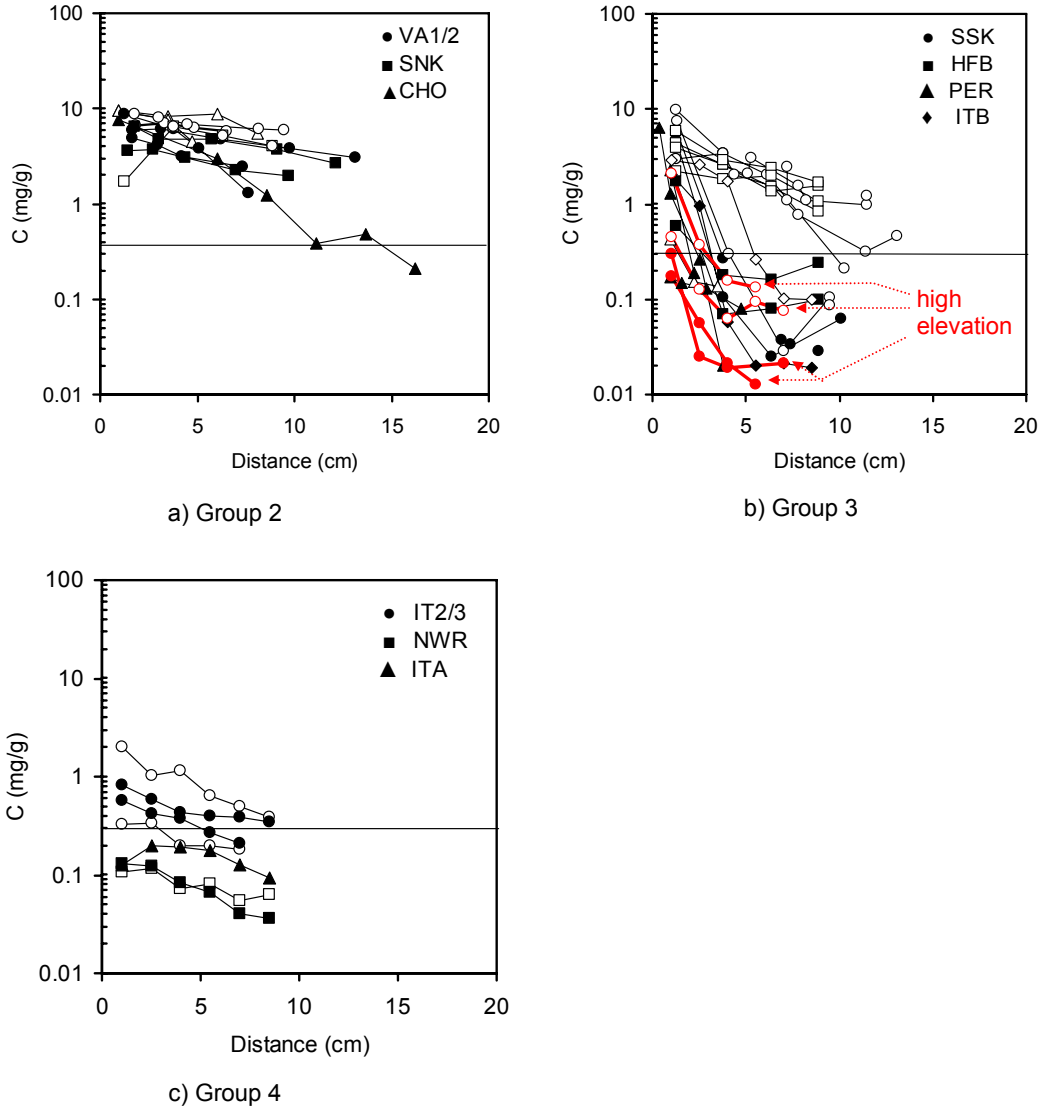

Figure 9. Chloride penetration profiles. Solid symbols: sound concrete. Open symbols: cracked concrete. Thick line, arrowed: high elevation trestle cap SSK locations. Horizontal line: conservative chloride threshold value ~0.3 mg/g (C_T~0.7 kg/m^3). Numeric chloride profile data and core identification are given in the companion project BD544-31 Final Report, Appendix I [10].

Figure 10. Extensive corrosion damage (CH2)


Figure 11. Typical steel and undercoating condition in disbonded ECR extracted from SSK, showing minor rust at coating breaks, and nearby discoloration of the metal surface. Trestle cap beam, 7.5 m AHT (SSK 140E2).

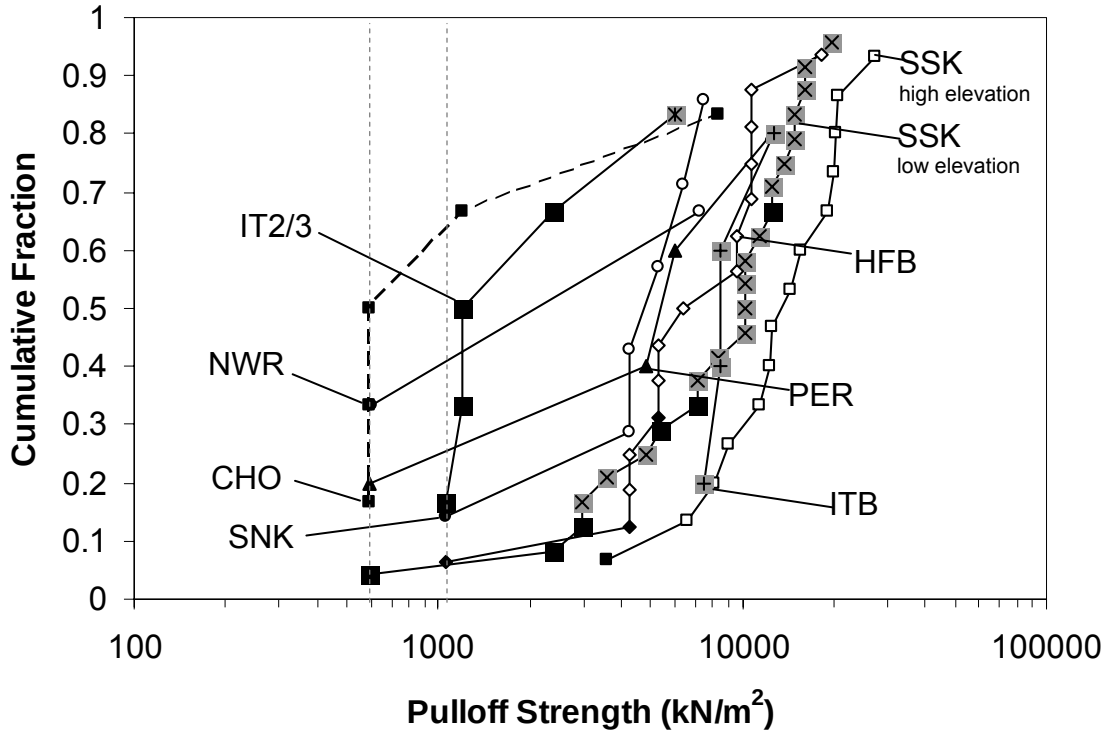

Figure 12. Epoxy coating pull-off strength. The pull-off strengths for Vaca Cut samples were negligible. Solid black symbols represent measured pull-off strengths. Other symbols represent lower bound pull-off strength failure at cyanoacrylate adhesive. Vertical lines represent minimum measurable strengths using metal dollys, nominal area 0.049 and 0.028 cm^2.

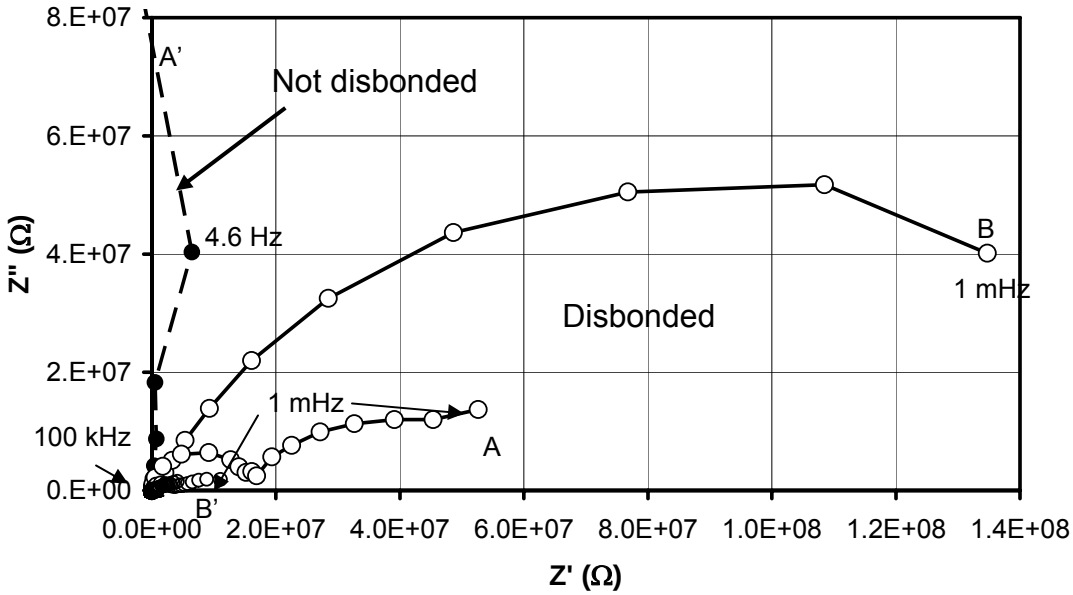

Figure 13. Impedance manifestation of disbondment. ECR from SSK high elevations. A,B Sound concrete core. A',B' Companion on crack core. (A, A': 140E2, 140E1. B, B':33W2, 33W1.)

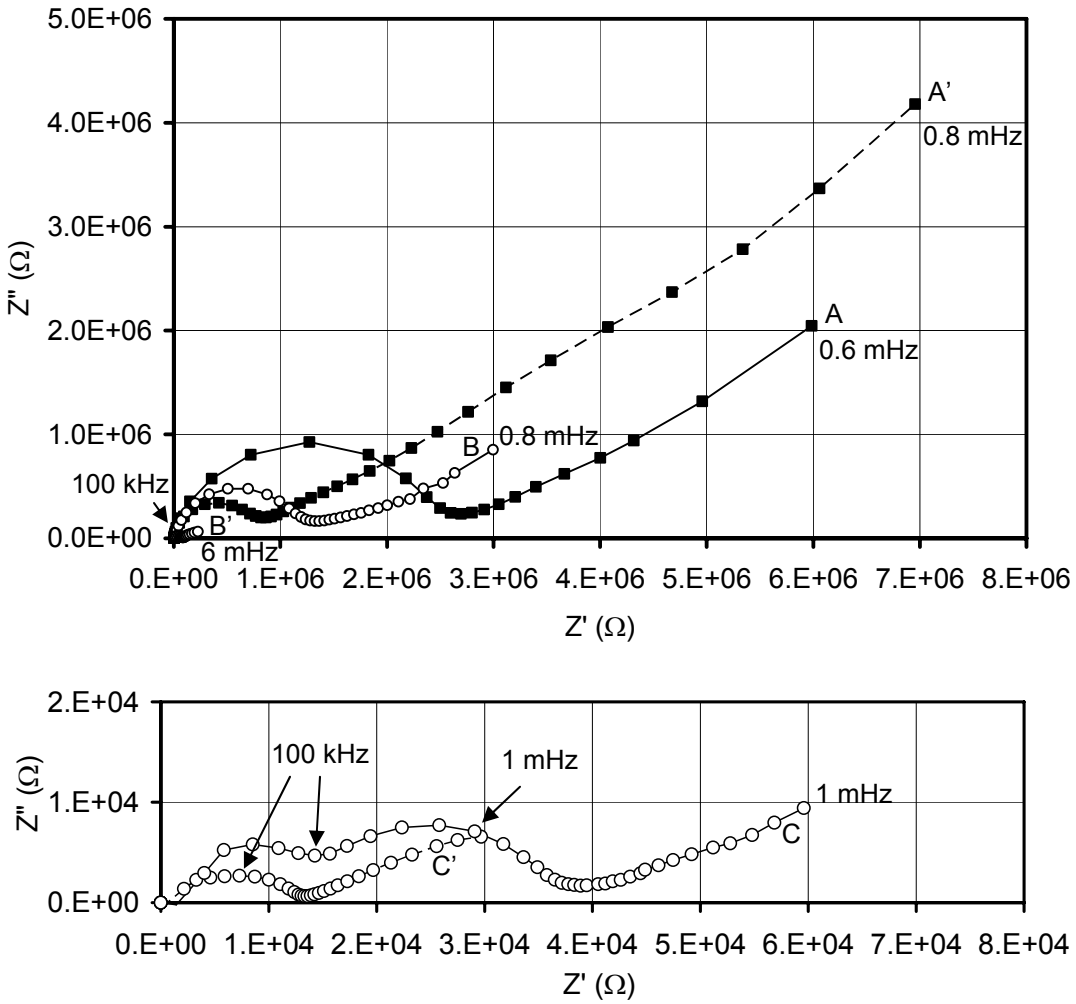

Figure 14. ECR Impedance manifestation of presence of a crack in the core (low elevation SSK samples). A,B,C Sound concrete core; A',B',C' Companion on-crack core; crack widths were 0.13, 0.25 and 0.23 mm respectively. (A, A':118W4,118W3. B, B': 118W2, 118W1. C,C': 117E3, 117E1).

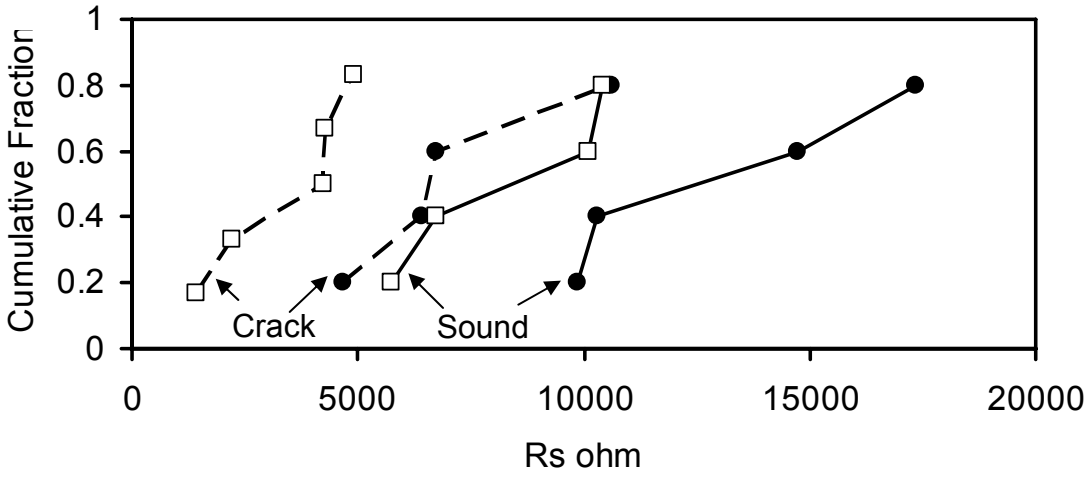

Figure 15. Solution resistance measured by EIS (SSK)
● High elevations. □ Low elevations

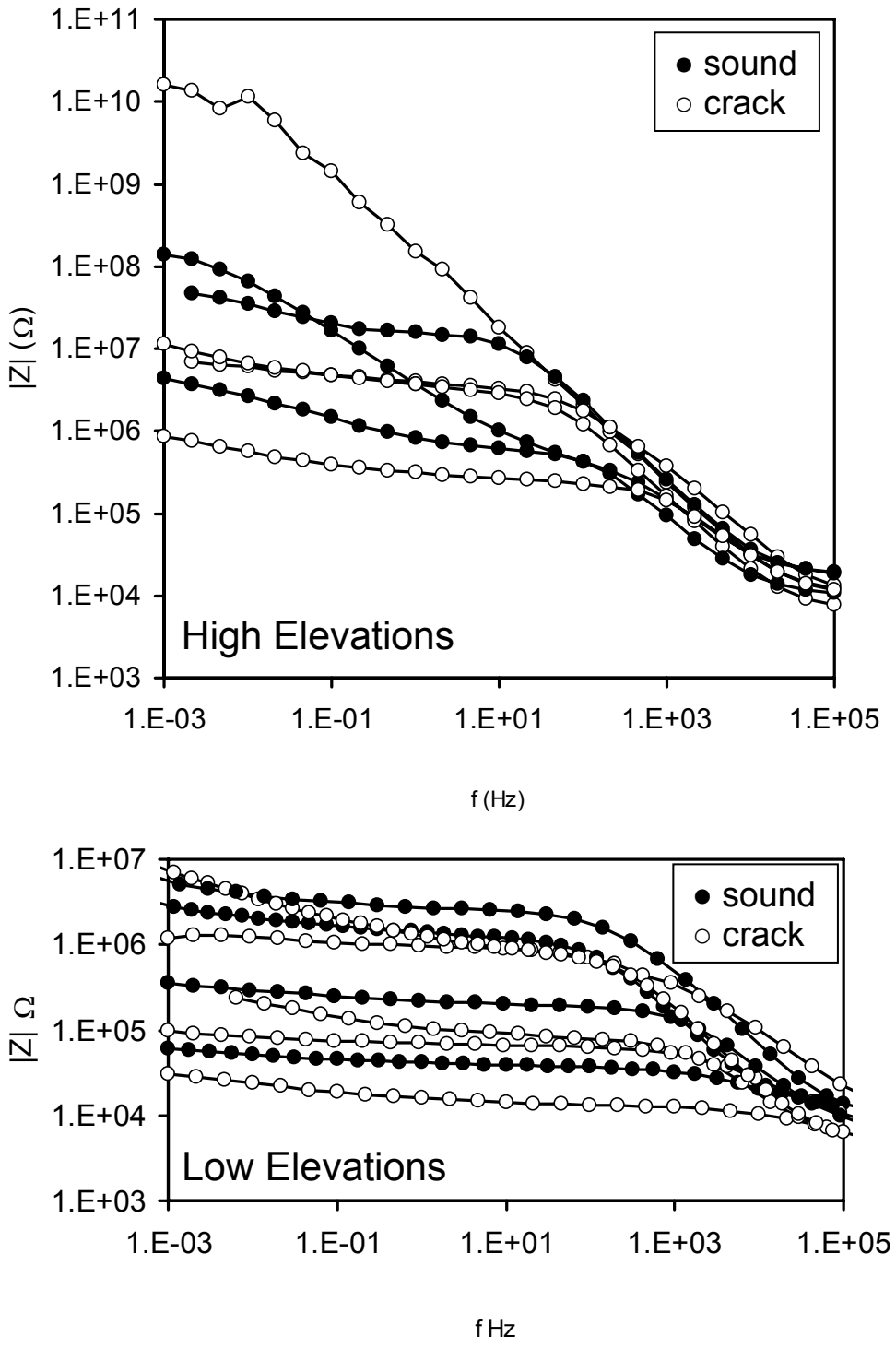

Figure 16. Comparison of impedance measurements of ECR from SSK, high and low elevations.

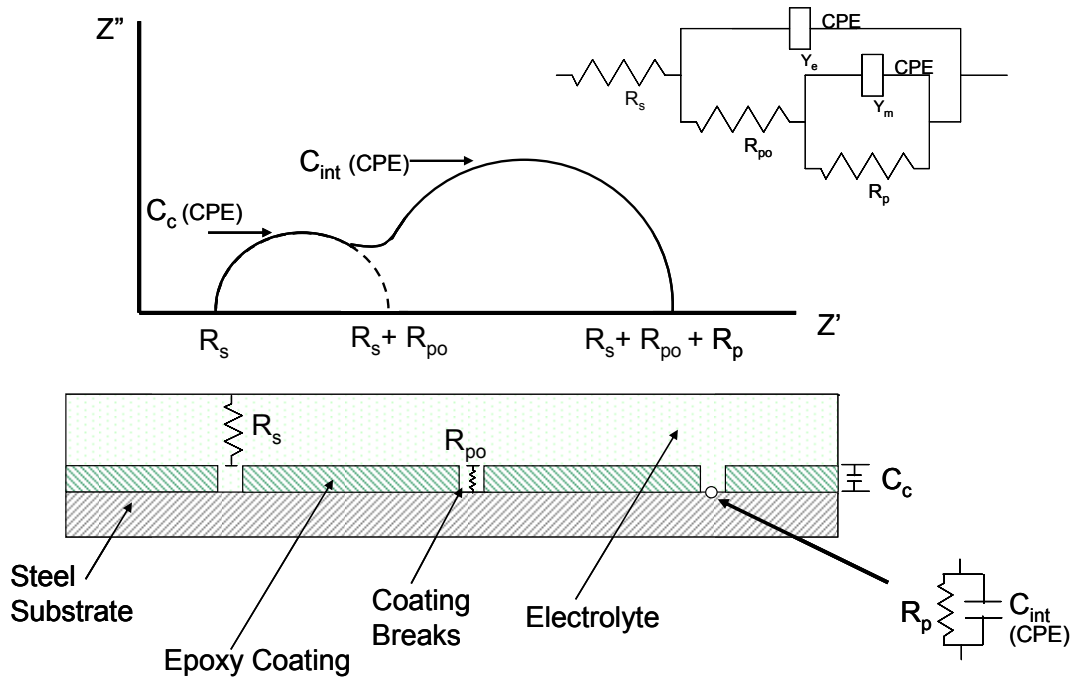

Figure 17. Idealized Impedance diagram of coated metal system with coating breaks and equivalent circuit analog.

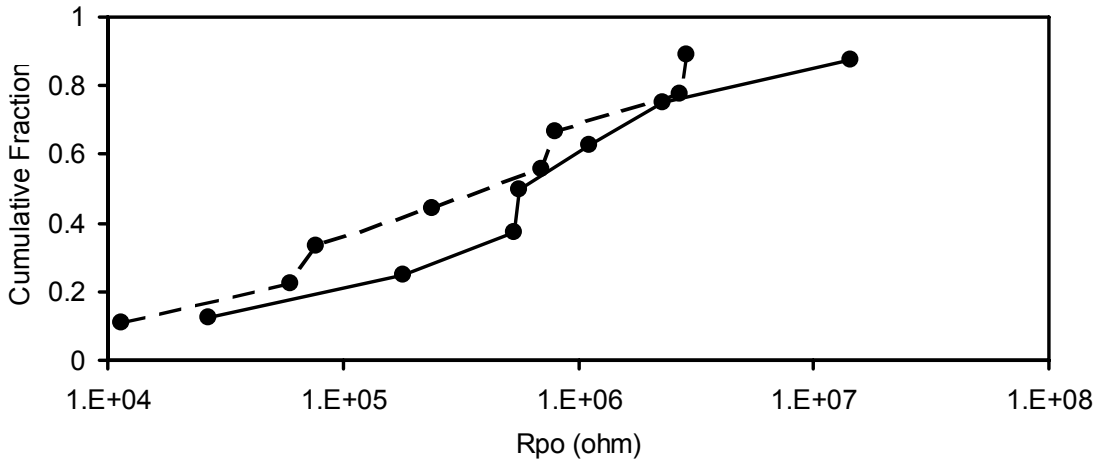

Figure 18. Pore resistance in ECR from SSK sound and cracked concrete locations. – sound concrete, -- cracked concrete.

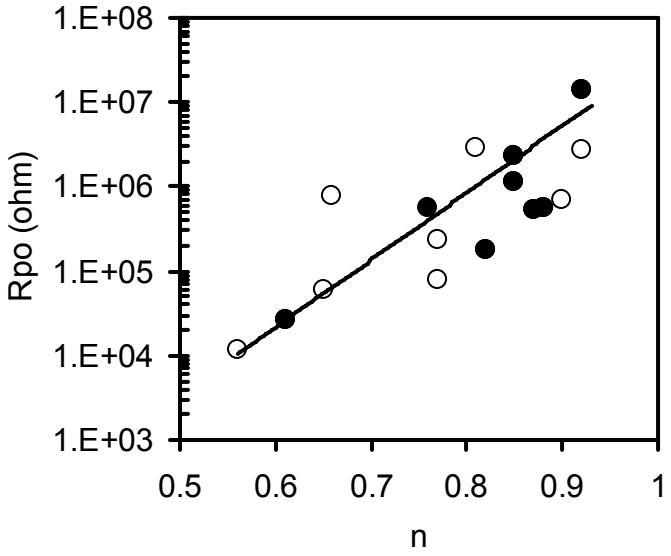

Figure 19. Correlation of R_{po} and n. (SSK)
●Sound concrete. ○ Cracked concrete.

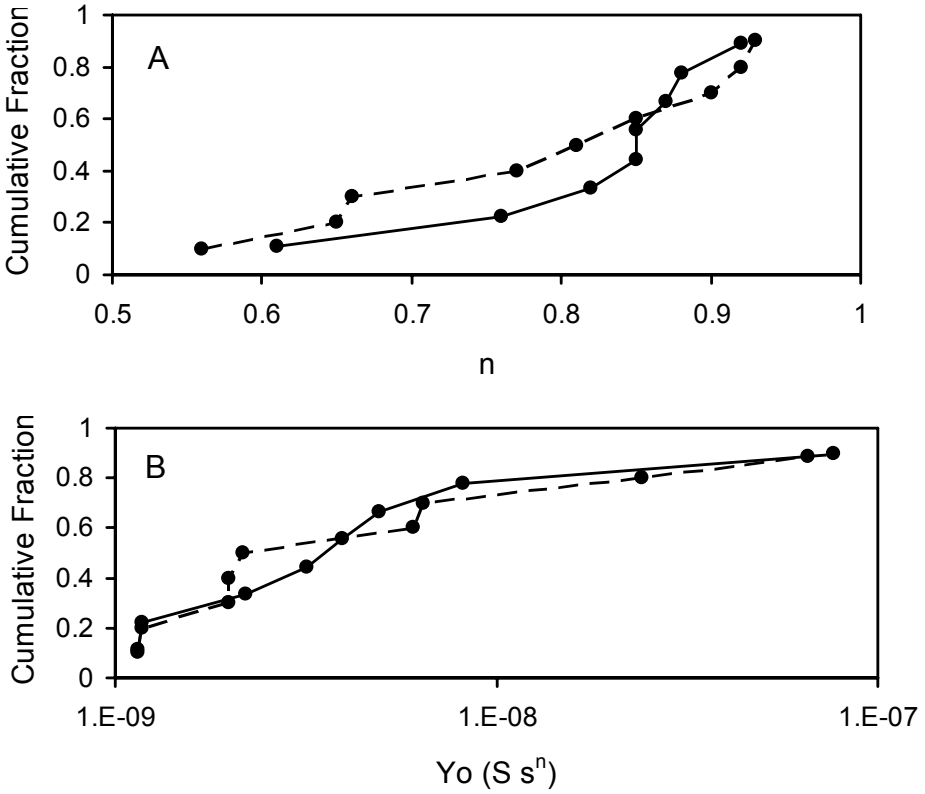

Figure 20. Cumulative fraction of coating CPE component values (SSK)
a) n and b) Y_o. – sound concrete, -- cracked concrete.

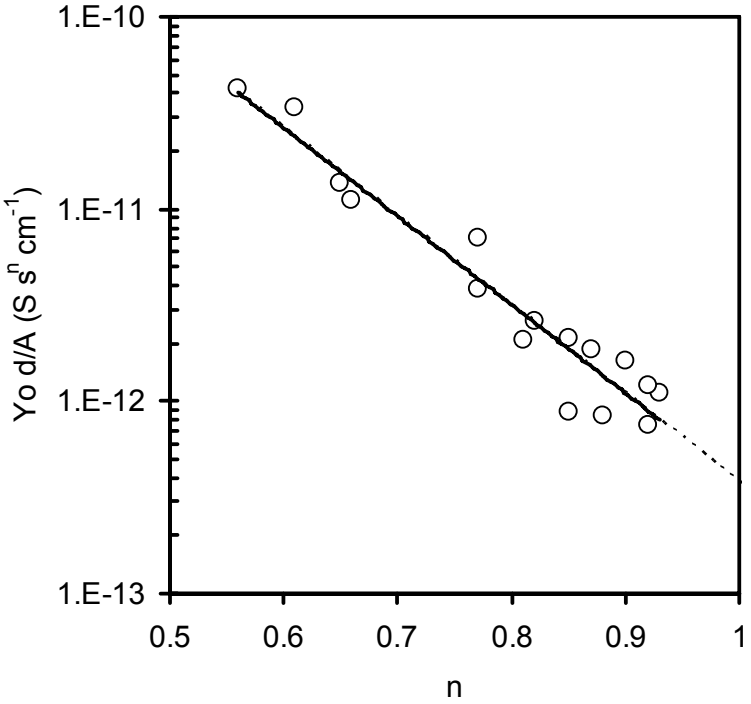

Figure 21. Correlation of Y_o and n for the coating CPE component (SSK).

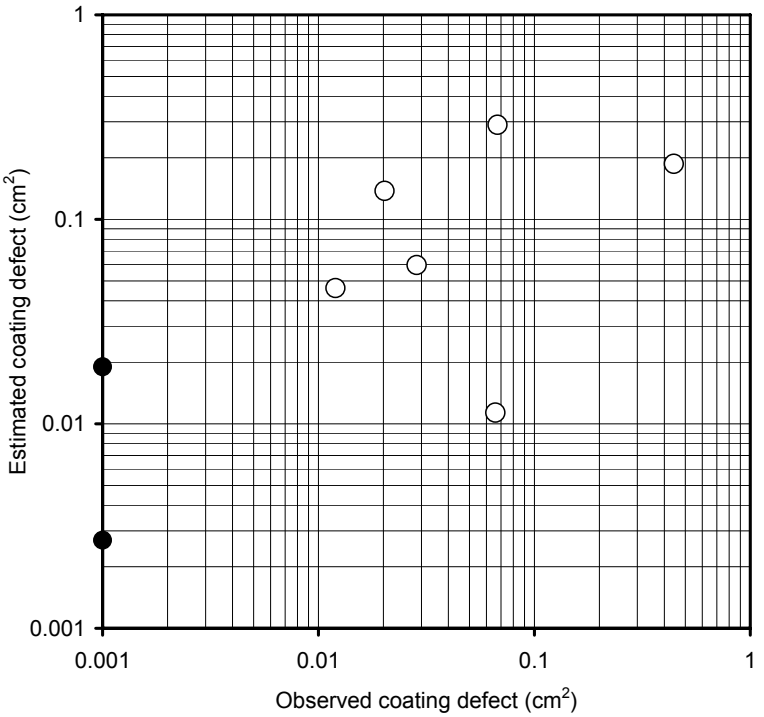

Figure 22. Comparison of observed coating defect area to estimated coating defect area (SSK). Solid symbol ● represents samples where no coating defects were observed but were assumed to be bound by a minimum detection limit, 0.001 cm^2.

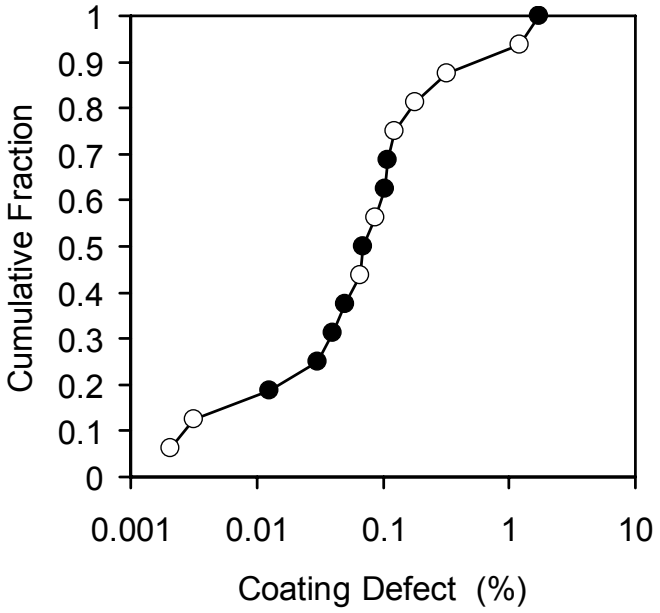

Figure 23. Cumulative fraction of coating defect as percentage of bar area (SSK) by direct observation (open symbol) or by estimation from impedance data (solid symbol).

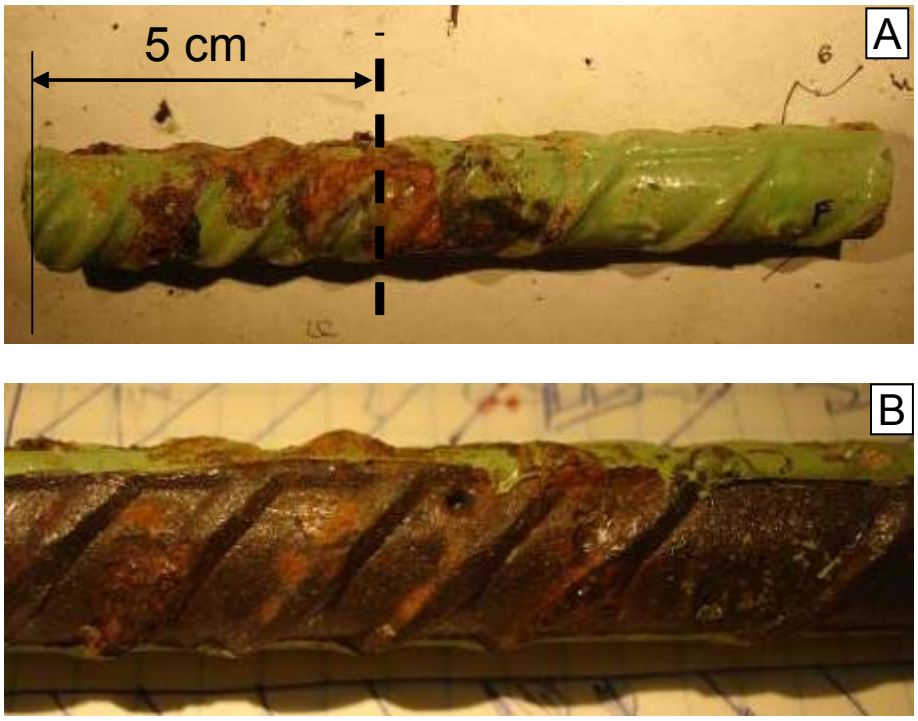

Figure 24. ECR corrosion at crack location (HFB59E1).
A. Corrosion products on bar surface. The line represents the location of the crack intersection. B. Appearance after partially removing the coating and exploring into the corrosion products.

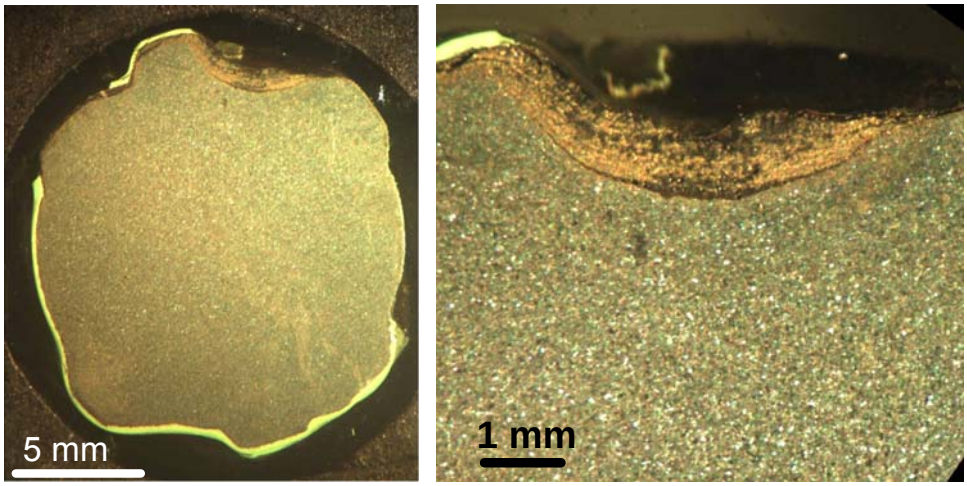

Figure 25. Cross section of ECR bar showing severe corrosion at a crack location of HFB59E1. Left: Entire Bar cross-section. Right: Close up of corrosion penetration.

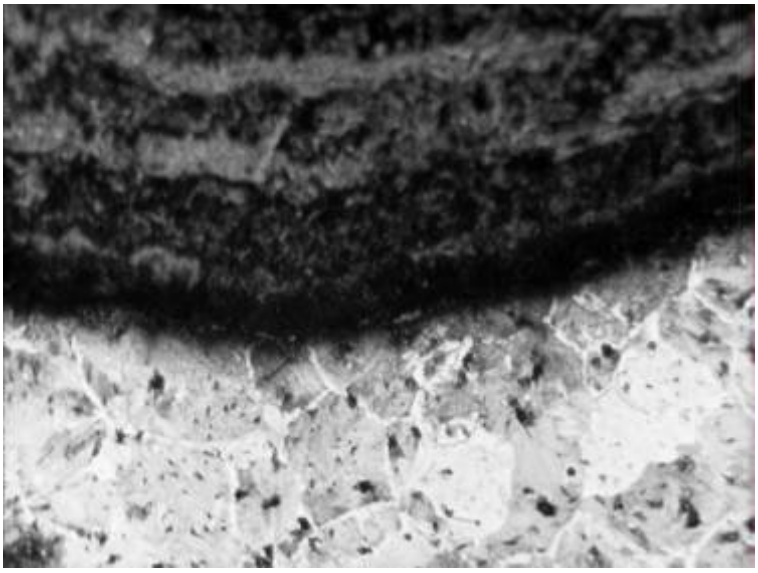

Figure 26. Corrosion product - base metal interface showing progression of corrosion into the microstructure of the rebar steel (HFB59W1).

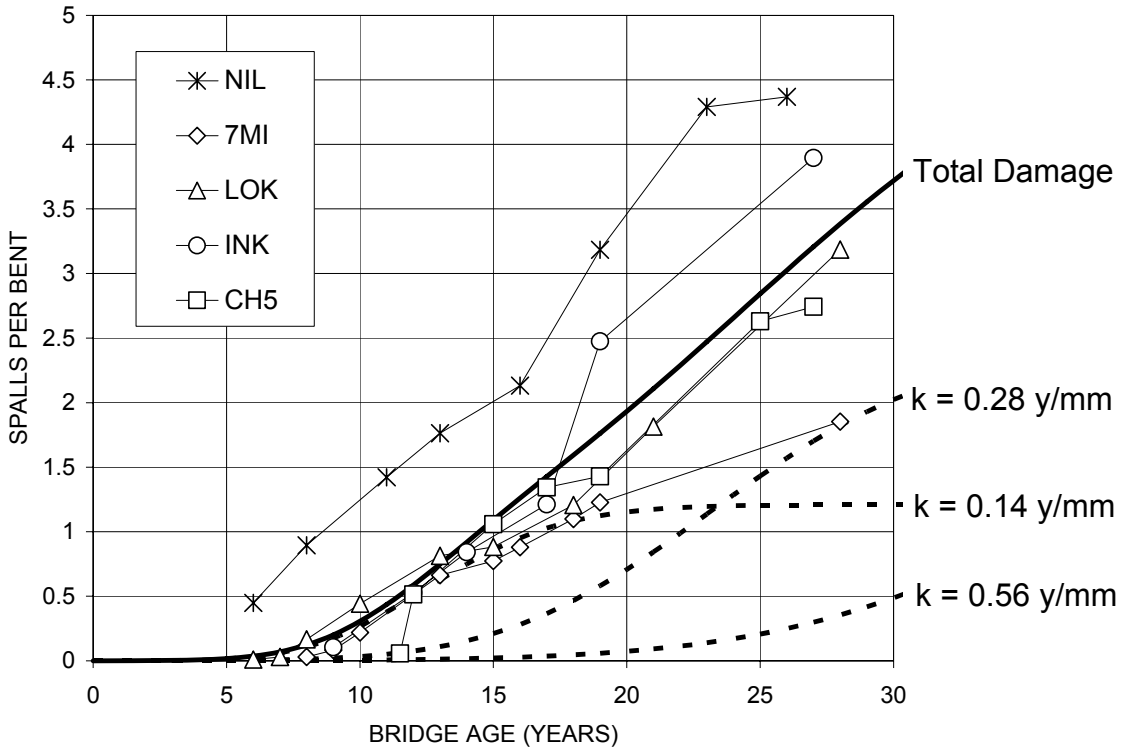

Figure 27. Projected damage function for Group 1 bridges. Thick bold line: total damage projection. Dashed lines: partial damage from each of the rebar assembly fractions considered;: 2% of the rebar with k=0.14 y/mm; 4% with k=0.28 y/mm and 8% with k=0.56 y/mm.

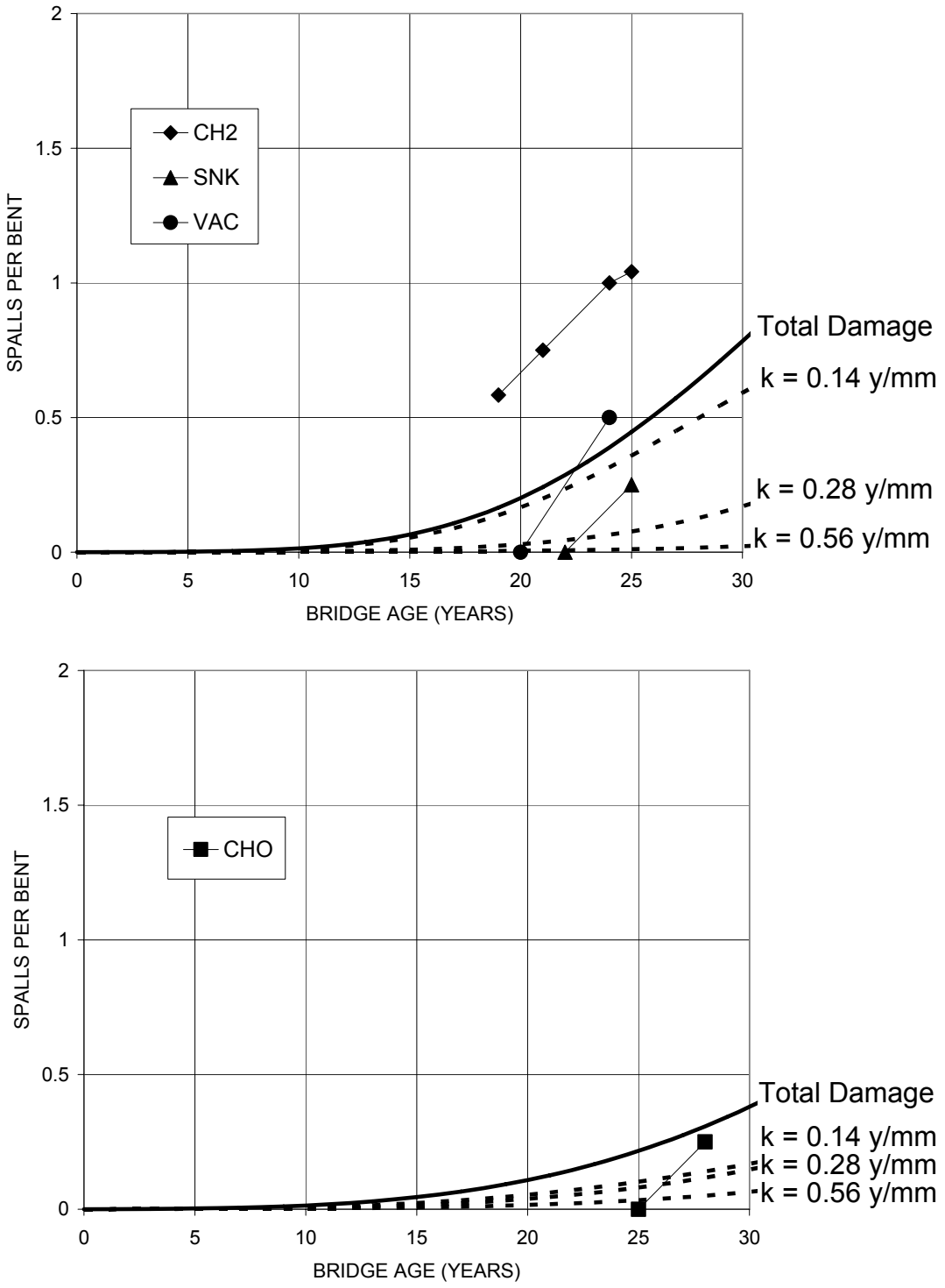

Figure 28. Projected damage function for Group 2 bridges. Thick bold line: total damage projection. Dashed lines: partial damage from each of the rebar assembly fractions considered; 2% of the rebar with k=0.14 y/mm; 4% with k=0.28 y/mm and 8% with k=0.56 y/mm.

Figure 29. Projected damage function for Group 3 bridges. Thick bold line: total damage projection. Dashed lines: partial damage from each of the rebar assembly fractions considered; 2% of the rebar with k=0.14 y/mm; 4% with k=0.28 y/mm and 8% with k=0.56 y/mm.

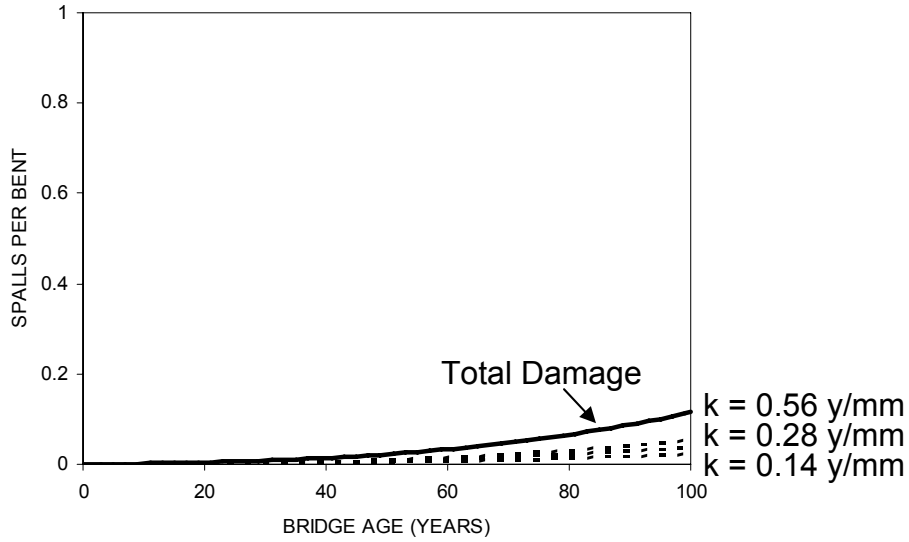

Figure 30. Projected damage function for Group 4 bridges. Thick bold line: total damage projection. Dashed lines: partial damage from each of the rebar assembly fractions considered; 2% of the rebar with k=0.14 y/mm; 4% with k=0.28 y/mm and 8% with k=0.56 y/mm.

APPENDIX

Table A1. ECR Open-circuit Potential Field Data.

	Bridge Name	Location	Elevation AHT (m)							Open-Circuit Potential (mV_{CSE})						
			A	B	C	D	E	F	G	A	B	C	D	E	F	G
Group 2	VA1/2	2A	S†	0.3	0.46	0.61	0.91	1.22		-524	-499	-487	-480	-443	-402	
			S†	0.3	0.46	0.61	0.91	1.22		-542	-516	-507	-501	-478	-420	
			S†	0.3	0.46	0.61	0.91	1.22		-580	-563	-556	-540	-508	-451	
			S†	0.3	0.46	0.61	0.91	1.22		-511	-499	-496	-482	-448	-403	
		3B	S†	0.3	0.46	0.61	0.91	1.22	1.68	-547	-468	-461	-412	-363	-293	-279
			S†	0.3	0.46	0.61	0.91	1.22	1.68	-517	-445	-407	-380	-334	-280	-349
			S†	0.3	0.46	0.61	0.91	1.22	1.68	-596	-523	-493	-459	-408	-354	-160
	SNK	8A	S†	-0.1	0	0.2	0.4	0.6	0.8	-665	-627	-658	-648	-628	-637	-607
			1.0	1.1	1.2	1.4	1.6	1.8	1.9	-578	-534	-543	-469	-464	-366	-309
			S†	-0.1	0	0.2	0.4	0.6	0.8	-665	-628	-652	-615	-628	-620	-618
			1.0	1.1	1.2	1.4	1.6	1.8	1.9	-603	-581	-551	-464	-435	-324	-290
		9B	S†	0	0.3	0.61	0.91	1.22	1.52	-584	-556	-578	-552	-511	-463	-421
			S†	0	0.3	0.61	0.91	1.22	1.52	-581	-543	-575	-521	-503	-449	-416
Group 3	SSK	18	0.8	1.1	1.4	1.7	2.0	2.3	2.6	-475	-482	-443	-440	-438	-342	-349
			2.9							-339						
		117	S†	-0.3	0	0.3	0.6	0.9	1.2	-612	-612	-615	-583	-577	-239	-226
			1.5	1.8	2.1					-172	-180	-69				
		118	S†	0	0.3	0.6	0.9	1.2	1.5	-245	-242	-256	-263	-283	-276	-259
			S†	0	0.3	0.6	0.9	1.2	1.5	-178	-170	-168	-185	-196	-199	-209
		33	7.7							-379						
			7.7							-303						
		84	7.5	7.6						-445	-379					
			7.5	7.6						-191	-313					
		140	7.4	7.5						-94	-127					
			7.4	7.5						-71	-104					
		143	7.3	7.3						-487	-264					
			7.3	7.3						-378	-181					
		167	7.2							-172						
			7.2							-144						
	HFB	52N	0	0.15	0.3	0.45	0.61			-375	-451	-470	-414	-428		
		55W	0	0.15	0.3	0.45	0.61	0.76	0.91	-258	-294	-306	-300	-320	-340	-367
			1.1	1.2						-305	-335					
		59W	S†	-0.5	-0.3	-0.1	0.1	0.3	0.5	-524	-588	-581	-557	-484	-462	-411
			0.7							-687						
	PER	26	S†	0	0.15	0.3	0.45	0.61	0.76	-648	-603	-484	-412	-346	-284	-266
			0.9	1.1	1.2	1.4	1.5			-303	-247	-235	-223	-183		
			S†	0	0.15	0.3	0.45	0.61	0.76	-656	-622	-504	-407	-355	-295	-258
			0.9	1.1	1.2	1.4	1.5			-296	-225	-185	-211	-144		
	ITB	B	S†	0.1	0.2	0.3	0.4	0.5	0.6	-77	-180	-179	-218	-144	-112	-80
			0.7	0.8	0.9	1.0	1.1	1.2		-90	-84	-76	-104	-61	-71	
Group 4	ITA	D	S†	0	0.1	0.2	0.3	0.4	0.5	-201	-327	-345	-368	-362	-365	-362
			0.7	0.8	0.9	1.0				-263	-271	-250	-251			
	IT2	B	S†	0.4	0.5	0.6	0.7	0.8	0.9	-589	-627	-614	-545	-530	-	-274
			1.0	1.1	1.2	1.3				-236	-356	-103	-119			
			S†	0.4	0.5	0.6	0.7	0.8	0.9	-574	-447	-370	-383	-387	-353	-151
			1.0	1.1	1.2	1.3				-146	-122	-118	-113			
	IT3	C	S†	0.1	0.2	0.3	0.4	0.6	0.7	-416	-	-522	-526	-521	-398	-400
			0.8	0.9	1.0	1.1	1.2			-344	-285	-229	-259	-41		
			S†	0.1	0.2	0.3	0.4	0.6	0.7	-467	-470	-479	-467	-461	-404	-352
			0.8	0.9	1.0	1.1	1.2			-324	-397	-383	-361	-333		

† Submerged region.

Additional detailed information on core extraction location and specimen identification is given in the companion Project BD544-31 Final Report [10].